https://doi.org/10.5194/egusphere-2024-3713
Preprint. Discussion started: 13 December 2024

The future North Atlantic jet stream and storm track: relative contributions from sea ice and sea surface temperature changes

Daniel Köhler[1], Petri Räisänen[2], Tuomas Naakka[2, 3], Kalle Nordling[2], and Victoria A. Sinclair[1]

[1]Institute for Atmospheric and Earth System Research/Physics, Faculty of Science, P.O. Box 64, University of Helsinki, 00014 Helsinki, Finland
[2]Finnish Meteorological Institute, Helsinki, Finland
[3]Department of Meteorology and Bolin Centre for Climate Research, Stockholm University, Stockholm, Sweden

Correspondence: Daniel Köhler (daniel.kohler@helsinki.fi)

Abstract. Using a novel set of coordinated simulations with four different models, the response of the wintertime (December - February) North Atlantic jet stream and storm track to prescribed sea surface temperatures and sea-ice loss is analysed. Three out of the four models show a southward shift of the upper-level jet stream with an increase in jet speed over Europe, where the contribution of sea surface temperatures dominates over the effects of sea-ice loss. However, the remaining model lacks the increase in jet speed over Europe, which originates from opposite responses of similar magnitude due to the future sea surface temperatures and sea-ice cover. The jet stream responses are primarily driven by the change in the meridional temperature gradient and, as a consequence, baroclinicity. At the same time, momentum flux convergence acts as a secondary amplifying and dampening factor. The same three models see a significant eastward shift of the extratropical cyclone track density, which is equally driven by changes to sea surface temperatures and sea ice cover. A consistent feature across all models is a decrease in the frequency of extratropical cyclones in the Mediterranean. The responses of extratropical cyclones to future sea-ice cover and sea surface temperatures do not exceed the inter-model climatological differences. Notable differences in the future response occur, and thus considerable uncertainty remains in how the European climate will respond to a warmer climate.

1 Introduction

Global warming due to rising greenhouse gas concentrations is accompanied by a warming of the average sea surface temperatures (SSTs) and loss of sea ice cover (SIC). In particular, the Arctic is severely impacted as it is currently warming up to 4 times faster than the global average, a phenomenon known as Arctic Amplification (Rantanen et al., 2022), and is experiencing dramatic sea-ice loss (Simmonds and Li, 2021). The sea-ice loss majorly contributes to a locally enhancing warming and moistening of the lower troposphere (Screen and Simmonds, 2010). However, the effects of sea-ice loss on the mid-latitude circulation is a topic of intense debate (Smith et al., 2022; Screen et al., 2022; Ye et al., 2023).

Mid-latitude weather is characterised by extratropical cyclones (ETCs), which are organised into storm tracks on climatological timescales. Another prominent atmospheric feature in the mid-latitudes is the eddy-driven jet stream, which acts as a guide for ETCs. It is critical to study together the storm track and the jet stream, as they are closely connected. Few previous studies have considered the jet and the storm track together, notable exceptions being Athanasiadis et al. (2010) and Ye et al.

https://doi.org/10.5194/egusphere-2024-3713
Preprint. Discussion started: 13 December 2024

(2023). The response of the North Atlantic jet stream to a warmer climate shows considerable inter-model variability over Europe (Oudar et al., 2020). Moreover, future changes to SSTs and SIC have been shown to have opposing influences on the jet stream. A poleward shift of the jet stream is associated with rising SSTs, meanwhile, SIC loss leads to an equatorward shift (Barnes and Screen, 2015; Screen et al., 2018). A similar pattern has been reported for the storm tracks (Yu et al., 2023). In particular, the North Atlantic jet response to sea ice is highly uncertain (Screen et al., 2018), espescially in the Northern Hemisphere winter (Simpson et al., 2014). Furthermore, the sea-ice loss-related changes to the storm tracks are tightly linked to the jet stream changes (Ye et al., 2023), and necessitating more studies simultaneously investigating jet stream and storm track changes.

A major source of uncertainty in future projections from fully coupled climate models is the differing amount of sea-ice loss that different models predict (Notz and Community, 2020). Moreover, the region and magnitude of sea-ice loss also has been shown to have a substantial impact on the atmospheric response. McKenna et al. (2018) showed moderate sea-ice loss in the Atlantic (Pacific) sector leads to a negative (positive) Arctic Oscillation response, meanwhile extensive sea-ice loss in either sector leads to a negative Arctic Oscillation response. The response of the mid-latitude tropospheric zonal wind, which is closely related to the jet stream, is proportional to the eddy momentum feedback. When constrained by observations of the eddy momentum feedback, it has been shown that models tend to underestimate responses of mid-latitude tropospheric zonal wind due to changes in SIC (Smith et al., 2022). It is important to note that the magnitude of the underestimation is strongly model-dependent. This limits the attribution of mid-latitude changes to differences in sea-ice loss or model representation of the atmosphere. To reduce the impact of different models' biases on the future response from future projections, numerous models are often used. However, this often limits studies to the use of multimodel means, which reduces the physical interpretability of future climate responses. On the other hand, studies focusing on the physical mechanism tend to employ one model, which have reduced accountability for modelling-related uncertainties (Levine et al., 2021; Dai and Song, 2020; Chemke et al., 2019).

This work aims to determine the wintertime response of the North Atlantic jet stream and storm track to changes in sea ice cover and sea surface temperatures and quantify their contributions to future climate conditions. This is achieved by exploiting coordinated experiments with four atmospheric general circulation models which are forced with the same prescribed SST and SIC, produced by "Climate Relevant interactions and feedbacks: the key role of sea ice and Snow in the polar and global climate system" (Naakka et al., 2024; CRiceS). The individual contributions are obtained by leveraging the power of the full set of experiments (historical climate, future SIC, future SST, and future SST+SIC — discussed further in section 2.1), each encompassing a continuous 40-year simulation. Prescribing either future SIC or SST while keeping the other at historical levels allows study the contributions of changes in SIC and SST in isolation, which is a limitation of fully-coupled climate simulations like CMIP6. Furthermore, by analysing carefully designed simulations from a relatively limited number of models, rather than all models from the CMIP6 archive, enables to reduce current uncertainties of the responses due to difference in projected SIC and SST and understand their underlying physical mechanisms. Specifically, this paper investigates the following questions:

- How well do the four models agree on the climatologies of the historical climate simulation when SSTs and sea ice cover are identical? The focus is on the winter North Atlantic jet stream, storm track and individual extratropical cyclones.

https://doi.org/10.5194/egusphere-2024-3713
Preprint. Discussion started: 13 December 2024

- Are there differences across models in the total future climate response when SSTs and sea ice cover are changed simultaneously?
- What are the relative contribution of SST and sea-ice cover changes to the total future climate response for each individual model? In particular, do the contributions oppose or amplify each other?

The study is structured as follows. Section 2 presents the conducted model simulations and introduces the metrics used to study the North Atlantic jet stream and storm track. Section 3 compares the North Atlantic jet stream and storm track across models in current climate conditions. Section 4 addresses the response of the North Atlantic jet stream in future climate and the contribution of SST and SIC. The physical mechanisms underlying the responses are explored in Section 5. Section 6 focusses on the responses to ETCs, including the contribution of SSTs and SIC. Specifically, it investigates the storm track density and multiple important ETC specific metrics like lifetime, maximum intensity and more. The study is concluded in Section 7.

2 Data and methods

2.1 Models and simulations

This study utilises a set of simulations by the CRiceS consortium, consisting of atmosphere-only simulations by four atmospheric general circulation models (OpenIFS-43r3, EC-Earth3, CESM2, and NorESM2). The conducted simulations were designed with the aim of studying the impacts of changes in sea surface temperatures (SSTs) and sea ice cover (SIC). This is achieved by running experiments prescribing different combinations of historical and future SIC and SSTs. The SST and SIC boundary conditions are obtained from the Australian Earth system model ACCESS-ESM1.5 from the CMIP6 archive (Eyring et al., 2016). ACCESS-ESM1.5 produces an Arctic sea ice cover evolution for the historical period that is in reasonable agreement with observations and provides the best guess estimate for future SIC (Notz and Community, 2020). Monthly climatological means from 1950 – 1969 are used as historical boundary conditions for the seasonal cycle, which is annually repeated. Meanwhile, the future boundary conditions use output from 2080 – 2099 under either the shared socioeconomic pathway SSP 1-2.6 or SSP 5-8.5 scenario. The full simulation set consists of a Baseline simulation (historical SST & SIC), two future simulations FT (future SST & SIC), two SST simulations $ftSST$ (future SST & historical SIC), and two SIC simulations $ftSIC$ (historical SST & future SIC). Each simulation was run for 40 years + 1 year of spin-up, starting on the 1st of January. The variables related to dynamics and thermodynamics are saved as 6-hourly output, enabling more diagnostics to be computed offline. A more detailed description of the models and simulations, including a basic meteorological analysis of temperature, mean sea level pressure, and precipitation, is found in Naakka et al. (2024).

This work analyses the 39 available complete Northern Hemisphere (NH) winters (DJF) using the SSP 5-8.5 FT, $ftSST$, $ftSIC$, and Baseline simulation. The analysis is limited to the North Atlantic (NA) sector defined as 95° W – 45° E and 20° N – 80° N with a focus on Europe (15° W – 35° E and 30° N – 70° N). The model output is vertically interpolated from model levels to isobaric surfaces from 1000 hPa to 50 hPa in 50 hPa intervals. The horizontal resolution is kept at the native resolution of each model. OpenIFS-43r3 and EC-Earth3 are run with TL255 horizontal resolution (0.7°x0.7° at the equator)

https://doi.org/10.5194/egusphere-2024-3713
Preprint. Discussion started: 13 December 2024

and 91 vertical model levels. NorESM2 has a longitude-latitude resolution of 2.5° x 1.9°, while for CESM2 the resolution is 1.25° x 0.9°. NorESM2 and CESM2 are run with 32 model levels.

2.2 Eddy-mean flow separation

The eddy-mean flow separation is a common technique to study synoptic-scale atmospheric dynamics. This is achieved by low-pass filtering using a 21-weight Lanczos filter with a 10-day cut-off period. The longer timescale of 10 days compared to the more common 6 days is motivated by including breaking synoptic waves as part of the eddy flow (Rivière et al., 2018). For the filtering, the shoulder months (November and March) are added to the data set and then subsequently discarded for analysis. The low-pass filter is applied to the potential temperature θ, and wind components u and v. The eddy part of the wind components u' and v' is determined by subtracting the low-pass filter field from the full field.

2.3 Baroclinicity and momentum flux convergence

The strength of the NA jet stream is predominantly governed by two physical mechanisms. One is the temperature gradient which leads to vertical changes in the wind speed described by the thermal wind law. Relevant for the jet stream is the meridional temperature gradient which is negative (e.g. temperature decreases towards the poles) in the troposphere, leading to the zonal wind increasing with height. The other mechanism originates from eddy-mean flow interaction, whereby the momentum of atmospheric waves (eddies) is fed back to the jet stream (Eliassen and Palm, 1961; Hoskins et al., 1983).

In isobaric coordinates, the horizontal temperature gradient is proportional to the potential temperature gradient, which is quantified by the meridional component of the baroclinicity vector B_y. The baroclinicity vector, $\boldsymbol{B}_s$, is given by

$$\boldsymbol{B}_s = -\frac{\nabla\bar{\theta}}{\sqrt{S}}, \text{ where } S = \frac{1}{h}\frac{\partial\bar{\theta}}{\partial p} \text{ and } h = \frac{R}{p}\left(\frac{p}{p_0}\right)^{R/c_p}, \tag{1}$$

as used by Cai and Mak (1990) and Schemm and Rivière (2019). $\boldsymbol{B}_s$ is calculated from the low-pass filtered potential temperature $\bar{\theta}$. Additionally, the temperature gradient $\nabla\bar{\theta}$ is normalised by the stability S, which uses the scale height h, which includes the gas constant for air R, specific heat capacity of air at constant pressure c_p, and reference pressure $p_0 = 1000$ hPa. The zonal wind speed and the Eady growth rate are proportional to the meridional component of the baroclinicity B_y.

Multiple approaches have been developed to characterise the eddy-mean flow interaction and its effects on the jet speed, most notable being the Eliassen-Palm flux (Eliassen and Palm, 1961) and E-vectors (Hoskins et al., 1983). The Eliassen-Palm flux uses the zonal averages and quantifies eddies as deviations from the zonal average. On the other hand, E-vectors utilise all 3 spatial dimensions, where the eddies and mean flow are obtained by using temporal filters (Sect. 2.2). Both methods are physically motivated by the transfer of momentum between eddies and mean flow. Thus, they share a similar mathematical form of the meridional and vertical components. The present article uses the meridional component F_ϕ of the E-vectors, defined as

$$F_\phi = a\,\cos\phi\,(-u'v')\,, \tag{2}$$

https://doi.org/10.5194/egusphere-2024-3713
Preprint. Discussion started: 13 December 2024

where a is the radius of Earth and ϕ is the latitude. The variables u' and v' symbolise eddy in terms of the horizontal wind components. Specifically, the momentum flux convergence

$$MFC = \left\langle \frac{1}{a\ \cos\phi} \frac{\partial F_\phi\ \cos\phi}{\partial \phi} \right\rangle \tag{3}$$

is calculated and results are interpreted by the zonal mean denoted by $\langle \cdot \rangle$. The momentum flux convergence MFC is proportional to the acceleration of the zonal wind speed u and quantifies the feedback of eddies on the jet.

While the temperature gradient and eddy-mean flow interaction mechanisms are not directly quantitively comparable, they are tightly connected in the jet stream area. This allows for a qualitative interpretation of compounding or opposing effect on the responses of the zonal wind due to sea ice and SST changes.

2.4 Extratropical cyclone tracking

Extratropical cyclones (ETCs) are objectively identified by the TRACK algorithm (Hodges, 1994 & 1999). The tracking is performed using mean sea level pressure as it is available as direct model output for all four models. The mean sea level pressure is truncated to T63 resolution with wave numbers 5 and lower removed, from which local minima are identified as ETCs. Like Priestley et al. (2023), the individual ETCs are filtered according to multiple criteria: they have to be (1) mobile (travel at least 1000 km), (2) long-lasting (have a lifetime of at least 48 hours), (3) affect Europe (at least 48 hours within the European box as defined in Sect. 2.1), and (4) and occur in the NH winter (genesis date in DJF).

Multiple quantities are derived from the TRACK output. Track count originates from the number of tracks, track duration is obtained from the number of timesteps, genesis latitude corresponds to the latitude at the first timestep, and latitudinal displacement is the difference in latitude between the last and first timestep. The mean speed is obtained by calculating the speed at each timestep from the change in coordinates and subsequently averaged over the track. The maximum intensity is the maximum of the negative pressure anomaly from the T63 mean sea level pressure within a single ETC track. The track density was computed using spherical kernels (Hodges, 1996) and estimates the likelihood that a given point is affected by an ETC.

2.5 Responses and significance testing

The responses are calculated as the difference of the December to February climatological means between a perturbed simulation and the Baseline simulation BL. The mathematical formulation is as follows:

$$\begin{aligned}
\Delta FT &= FT - BL, \\
\Delta SST &= ftSST - BL, \\
\Delta SIC &= ftSIC - BL, \\
\Delta NL &= FT - ftSST - ftSIC + BL.
\end{aligned} \tag{4}$$

The difference between the FT and Baseline climatology is referred to as Future response, denoted by ΔFT. The contribution of sea surface temperature, ΔSST, is calculated from the difference between the SST simulation $ftSST$ and Baseline simulation BL, and the sea ice contribution ΔSIC is calculated likewise. The summation of ΔSIC and ΔSST does not result in

https://doi.org/10.5194/egusphere-2024-3713
Preprint. Discussion started: 13 December 2024

ΔFT, leaving a non-linear term ΔNL, which is not shown in this paper. This non-linear term includes the lack of the effect of changed SSTs where sea ice is removed and resulting non-linear interactions. Furthermore, the different states of internal variability between the simulations also contribute to the non-linear term. For a more in-depth analysis of the residual term, consult Naakka et al. (2024).

To test if the climatological means of perturbed experiments are statistically different from the Baseline mean climatology, a two-tailed t-test with the 39 seasonal means for DJF as input is performed. A p-value above 0.05 is regarded as non-significant. Hence, in the Figures, areas without stippling show statistically significant responses.

3 Intercomparison of the Baseline simulation

This section compares the Baseline simulation across models. For readability, a detailed description of the Baseline simulation of OpenIFS-43r3 is given in each subsection. Subsequently, the key differences between the three remaining models and OpenIFS-43r3 are presented.

3.1 The horizontal perspective

The upper-level jet stream is a thin ribbon of high zonal wind speed u, identified at 250 hPa in this work. The subtropical jet stream is present over Northern Africa, however, the focus of this study is the North Atlantic (NA) jet stream, which originates at the North American east coast and ends over Europe. In OpenIFS-43r3 (Fig. 1a, colours), the NA jet stream shows a maximum between 36 $\mathrm{m\,s^{-1}}$ and 40 $\mathrm{m\,s^{-1}}$ above the Western NA. At the NA jet maximum, the jet is found around 30 °N – 40 °N and is broader than the jet's eastern end over Europe. Towards the east, the jet core moves northward, commonly referred to as the tilt of the NA jet. Meanwhile, the zonal wind speed in the jet core decreases gradually until it is only marginally higher compared to the westerly flow in the midlatitudes. The structure of the upper-level NA jet stream in the OpenIFS-43r3 Baseline simulation is in good agreement with what is found in reanalysis and coupled climate models (Harvey et al., 2020).

The baroclinicity B_y is diagnosed at 500 hPa. The maxima and minima in B_y closely coincide with the maxima and minima in u. In the NA (Fig. 1a, contours), the maximum in B_y is located slightly northward of the jet maximum, yet their respective shapes match closely. As was the case with the upper-level jet, B_y shows a northward tilt and an eastward decrease in magnitude.

Crucial to the storm tracks, the jet stream at lower levels is a feature in the zonal wind field u. It is detected using u at 850 hPa, which is commonly used in the context of the eddy-driven jet stream (Woollings et al., 2010). In OpenIFS-43r3, the lower-level jet is the strongest in the Central Atlantic (Fig. 2a, contours), which is east of the upper-level maximum. The maximum wind speeds lie between 9 $\mathrm{m\,s^{-1}}$ to 12 $\mathrm{m\,s^{-1}}$. Similar to the upper-level jet, the low-level jet shows a northward tilt from west to east.

The ETC track density is tightly linked to the presence of baroclinicity and the jet stream. Three strong maxima are identified (Fig. 2a, colours), one over the eastern USA, another at the North American East coast, and the last one south-east of Greenland. Generally, the ETC track density is highest in regions of high baroclinicity and on the northern flank of the lower-level and

https://doi.org/10.5194/egusphere-2024-3713
Preprint. Discussion started: 13 December 2024

upper-level jet stream, thus following the northward tilt across the NA. Further prominent features are elevated ETC track density in the Mediterranean and Baltic Sea. The ETC densities are in good agreement with reanalysis (Gramcianinov et al., 2020) and coupled climate models (Priestley et al., 2020).

Generally, the Baseline simulation from EC-Earth3 (Fig. 1b & Fig. 2b) is similar to that from OpenIFS-43r3 when the zonal wind speed at 250 hPa and at 850 hPa, baroclinicity, and ETC track density are considered. Minor differences are found in the ETC densities, which are 40 % higher in the north-eastern USA and mainland Europe compared to OpenIFS-43r3.

NorESM2 and CESM2 have comparable Baseline simulations to OpenIFS-43r3 and EC-Earth3. However, there are multiple distinguishing features. Most notably, the low-level jet stream is considerably faster, oriented more zonally, and the maximum shifted towards the east (Fig. 2c,d, contours) in both NorESM2 and CESM2 compared to OpenIFS-43r3 and EC-Earth3. Furthermore, the upper-level jet stream speed reduces more gradually towards the east, which results in higher jet speed over Europe (Fig. 1c,d, colours) in NorESM2 and EC-Earth3. Moreover, the ETC track density is higher extending from the North American East coast over the south-east of Greenland to Northern Europe (Fig. 2c,d, colours). Lastly, in NorESM2 and CESM2 the baroclinicity is lower outside the jet stream regions.

While NorESM2 and CESM2 share a similar pattern distinguishing the models from OpenIFS-43r3 and EC-Earth3, differences also exist between NorESM2 and CESM2. NorESM2 shows a 10 % stronger upper-level jet over Europe (Fig. 1c, colours) compared to CESM2 (Fig. 1d, colours). Another feature is in the ETC densities over Northern Europe, where CESM2 (Fig. 2d, colours) has higher values than NorESM2 (Fig. 2c, colours). This is related to higher ETC counts in CESM2 compared to NorESM2, which is discussed in Section 3.3.

3.2 The zonal cross-section perspective

In this part, the focus is shifted to the jet stream structure over Europe (30° N – 70° N, 15° W – 35° E), where the exit region of the NA jet stream is located. The left-hand side of the jet stream exit is an area which is favourable for extratropical cyclone development. The cross-sections of the zonal mean are utilised in Figure 3, where the zonal wind speed u (in colours), the baroclinicity B_y (in blue contours), and the eddy momentum flux convergence MFC (in black contours) are displayed. This allows insight into the European jet properties across models.

The OpenIFS-43r3 Baseline cross-section is presented in Figure 3a. The edge of the subtropical jet stream located over Northern Africa (around 30° N and 200 hPa) is visible as high values of u. A second maximum in zonal wind speed at 250 hPa and between 50° N and 60° N is associated with the jet exit region of the NA jet stream. The NA jet stream exit is a broad feature, with a maximum speed between 16 $\mathrm{m\,s^{-1}}$ and 18 $\mathrm{m\,s^{-1}}$. An area of increased baroclinicity B_y is found below and north of the NA jet maximum. The peak in B_y associated with the jet stream occurs between 600 hPa to 400 hPa. In addition, this NA jet stream maximum is co-located with a maximum in the eddy momentum flux convergence MFC, which contributes to the formation of the NA jet stream. EC-Earth3 (Fig. 3b) closely matches OpenIFS-43r3 in patterns and magnitudes of zonal wind speed u, baroclinicity B_y and eddy momentum flux MFC.

On the other hand, in CESM2 (Fig. 3d), the NA jet stream is a vertically deep feature, with a strong meridional gradient in wind speed and has a maximum speed between 22 $\mathrm{m\,s^{-1}}$ and 24 $\mathrm{m\,s^{-1}}$. The MFC with values between 100 $\mathrm{m^2\,s^{-2}}$ and 125

https://doi.org/10.5194/egusphere-2024-3713
Preprint. Discussion started: 13 December 2024

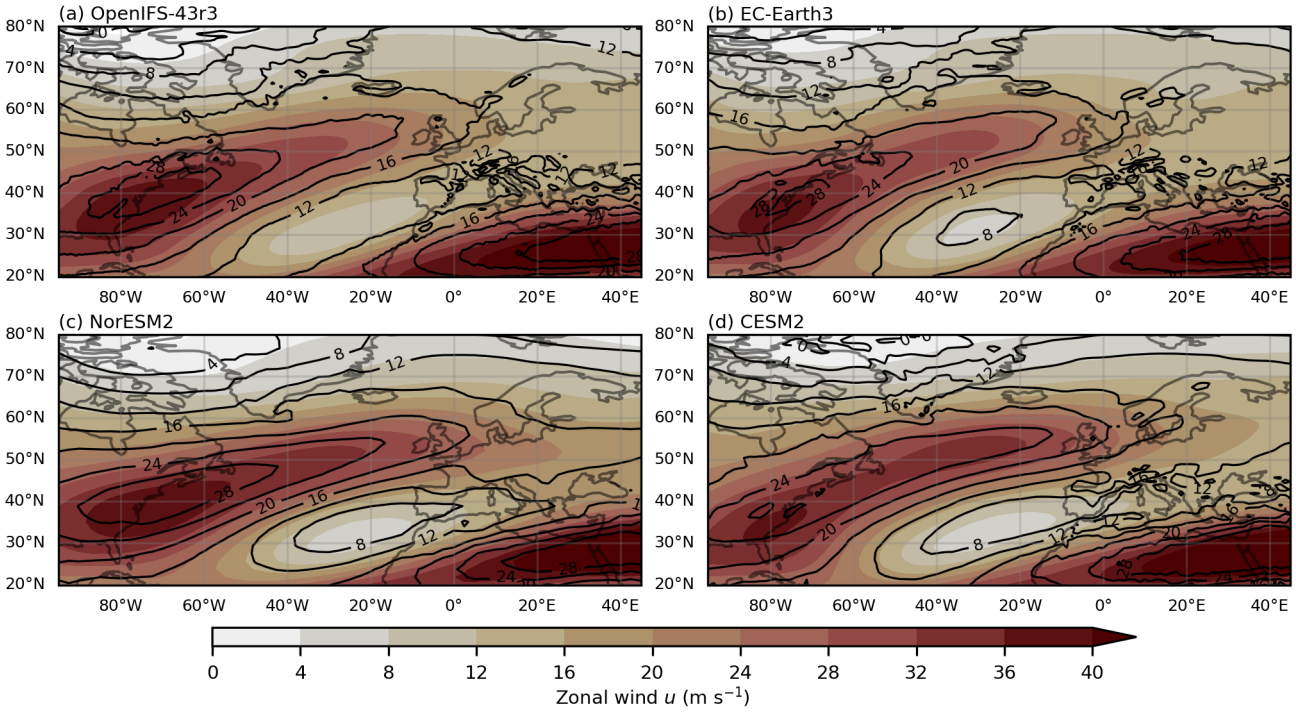

Figure 1. The 39-year DJF mean of zonal wind speed u at 250 hPa (in colour shading, $\mathrm{m\ s^{-1}}$) and baroclinicity B_y at 500 hPa (in black contours, $10^{-4}\ \mathrm{s^{-1}}$) for (a) OpenIFS-43r3, (b) EC-Earth3, (c) NorEMS2, and (d) CESM2.

$\mathrm{m^2\ s^{-2}}$ is considerably stronger compared to OpenIFS-43r3 and EC-Earth3. This indicates that the eddy-mean flow interaction contributes substantially to the jet structure in CESM2. Meanwhile, the baroclinicity exceeding $16{\cdot}10^{-4}\ \mathrm{s^{-1}}$ below the jet maximum is vertically thicker compared to OpenIFS-43r3 and EC-Earth3, which contributes to stronger jet maximum.

Lastly, NorESM2 (Fig. 3c) shares the vertically deep structure and a similar maximum NA jet speed as the CESM2 Baseline simulation. The baroclinicity shows small differences to CESM2, mainly a thicker layer exceeding $12{\cdot}10^{-4}\ \mathrm{s^{-1}}$ and $16{\cdot}10^{-4}\ \mathrm{s^{-1}}$ at the latitude of the NA jet. Most notably, NorESM2 has the highest values in MFC between 125 $\mathrm{m^2\ s^{-2}}$ and 150 $\mathrm{m^2\ s^{-2}}$). This emphasises the eddy-driven nature of the jet strength in NorESM2.

3.3 The ETC properties

Looking at the properties of ETCs affecting Europe (30° N – 70° N, 15° W – 35° E), Figure 4 provides insight into the ETC count, track duration, mean speed, maximum intensity, the genesis latitude, and latitudinal displacement. All models agree well on the distribution's overall shape and the range of values across all six ETC quantities. However, multiple statistically significant key differences in the mean values are addressed in the following. The detailed differences in the mean values are reported in Table A1 in the Appendix. For readability, the terms "significant" and "significantly" refer to a t-test with a significance threshold of 5%.

https://doi.org/10.5194/egusphere-2024-3713
Preprint. Discussion started: 13 December 2024

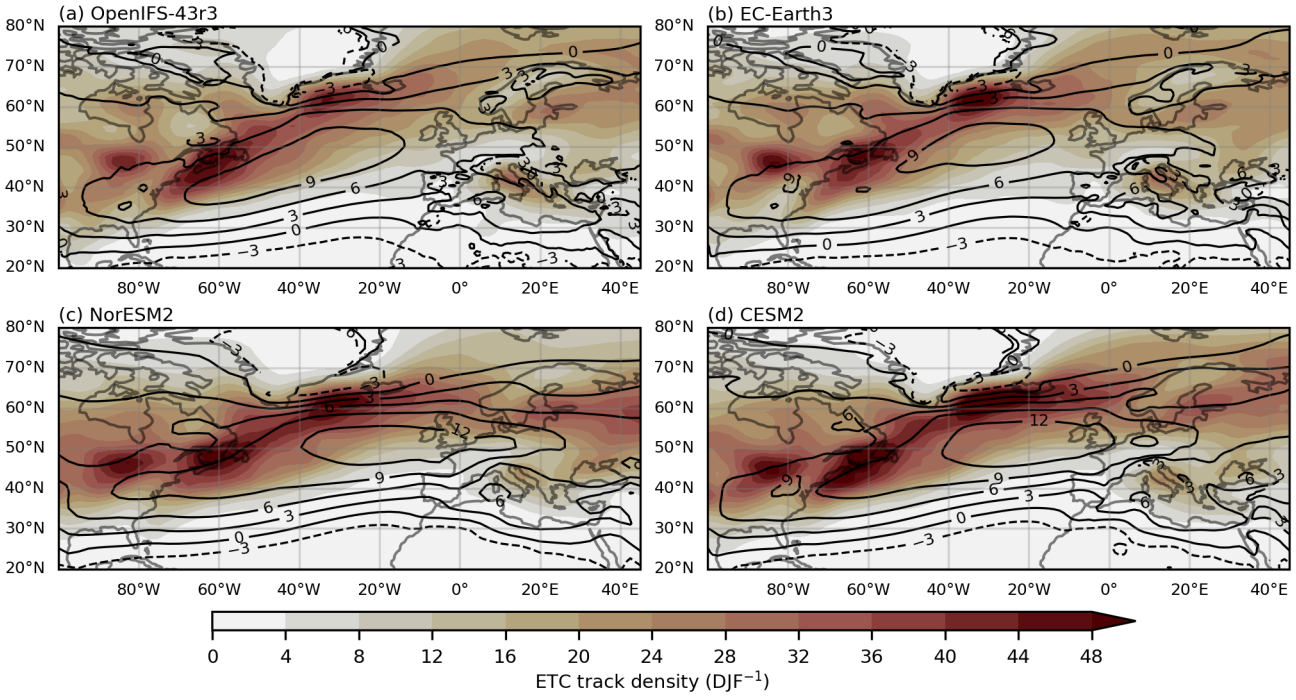

Figure 2. The 39-year DJF mean of ETC track density (in colour shading), zonal wind speed u at 850 hPa (in black contours, $\mathrm{m\,s^{-1}}$) for (a) OpenIFS-43r3, (b) EC-Earth3, (c) NorEMS2, and (d) CESM2. The ETC track density unit is number of ETCs per 5° spherical cap per winter season (DJF).

The most apparent differences are present in the ETC count. NorESM2 has a significantly lower number of ETCs affecting Europe (1550 total, 39.7 per winter season) than the 3 other models, while CESM2 has the highest number (1814 total, 46.5 per winter season). The mean values for OpenIFS-43r3 (1694 total, 43.4 per winter season) and EC-Earth3 (1720 total, 44.1 per winter season) are not statistically different from each other. Referring back to the track densities in Figure 2, the higher number of ETCs in CESM2 is the origin of the higher ETC track density compared to OpenIFS-43r3 and EC-Earth3. However, regardless of the lower ETC count in NorESM2, NorESM2 presents a higher ETC track density compared to OpenIFS-43r3 and EC-Earth3. This results from the combination of low mean speed and long lifetime of ETCs in NorESM2, which amplifies the ETC track density in the storm track.

The mean lifetime of ETCs is statistically different in each of the four models. This results in an order from the shortest to the longest lifetime: EC-Earth3 (120.6 h), OpenIFS-43r3 (124.9 h), CESM2 (132.5 h), NorESM2 (148.8 h). Next, in NorESM2, the mean speed of ETCs with a value of 11.0 $\mathrm{m\,s^{-1}}$ is significantly slower than in the other three models. EC-Earth3 has the fastest ETCs on average (11.9 $\mathrm{m\,s^{-1}}$). There is no statistical difference in mean speed between CESM2 (11.3 $\mathrm{m\,s^{-1}}$) and OpenIFS-43r3 (11.2 $\mathrm{m\,s^{-1}}$).

https://doi.org/10.5194/egusphere-2024-3713
Preprint. Discussion started: 13 December 2024

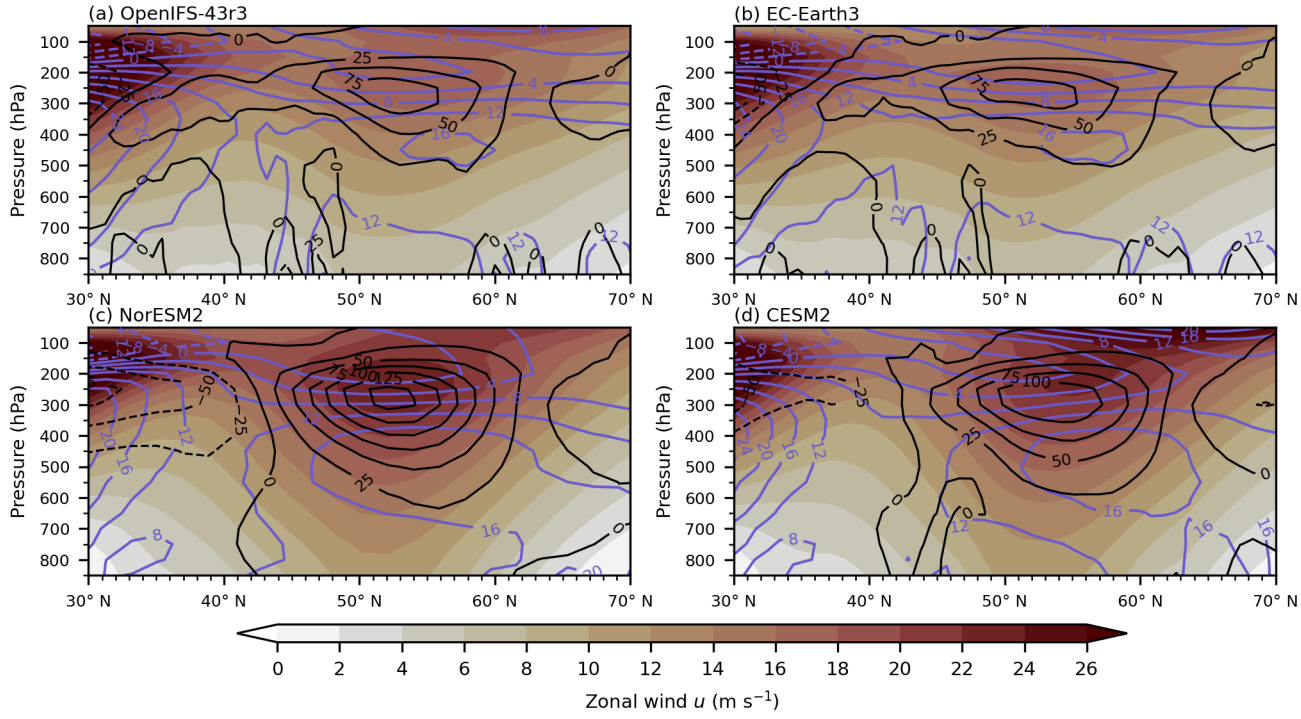

Figure 3. Zonal mean (15° W – 35° E) of the 39-year DJF mean of zonal wind speed u (in colour shading, $\mathrm{m\ s^{-1}}$), eddy momentum flux convergence MFC (in black contours, $\mathrm{m^2\ s^{-2}}$), and baroclinicity B_y (in blue contours, $10^{-4}\ \mathrm{s^{-1}}$) for (a) OpenIFS-43r3, (b) EC-Earth3, (c) NorEMS2, and (d) CESM2.

Furthermore, the mean maximum intensity is very similar in OpenIFS-43r3 (33.3 hPa), CESM2 (32.8 hPa), and NorESM2 (32.5 hPa) with no significant differences. EC-Earth3 is the exception, with a significantly higher mean maximum intensity of 35.3 hPa. Furthermore, CESM2 has significantly the most equatorward mean latitude of genesis of ETCs affecting Europe (39.4° N) among all four models. On the other extreme, EC-Earth3 has significantly the most poleward genesis (41.8° N). No significant difference is found between OpenIFS-43r3 (40.1° N) and NorESM2 (40.6° N). Lastly, latitudinal displacement is significantly different in all models, in order from least to most poleward: EC-Earth3 (12.8° N), OpenIFS-43r3 (14.0° N), CESM2 (15.1° N), NorESM2 (15.8° N).

4 The jet response to climate change

4.1 The total Future response of the jet

The response of the upper-level jet stream, quantified by the 250-hPa zonal wind speed, to changed SSTs and SIC (ΔFT) in the SSP5-8.5 scenario is shown in Figure 5. All models show an apparent deceleration on the poleward side of the subtropical jet stream over North Africa. This is due to an upward shift of the subtropical jet maximum visible in the vertical cross-

https://doi.org/10.5194/egusphere-2024-3713
Preprint. Discussion started: 13 December 2024

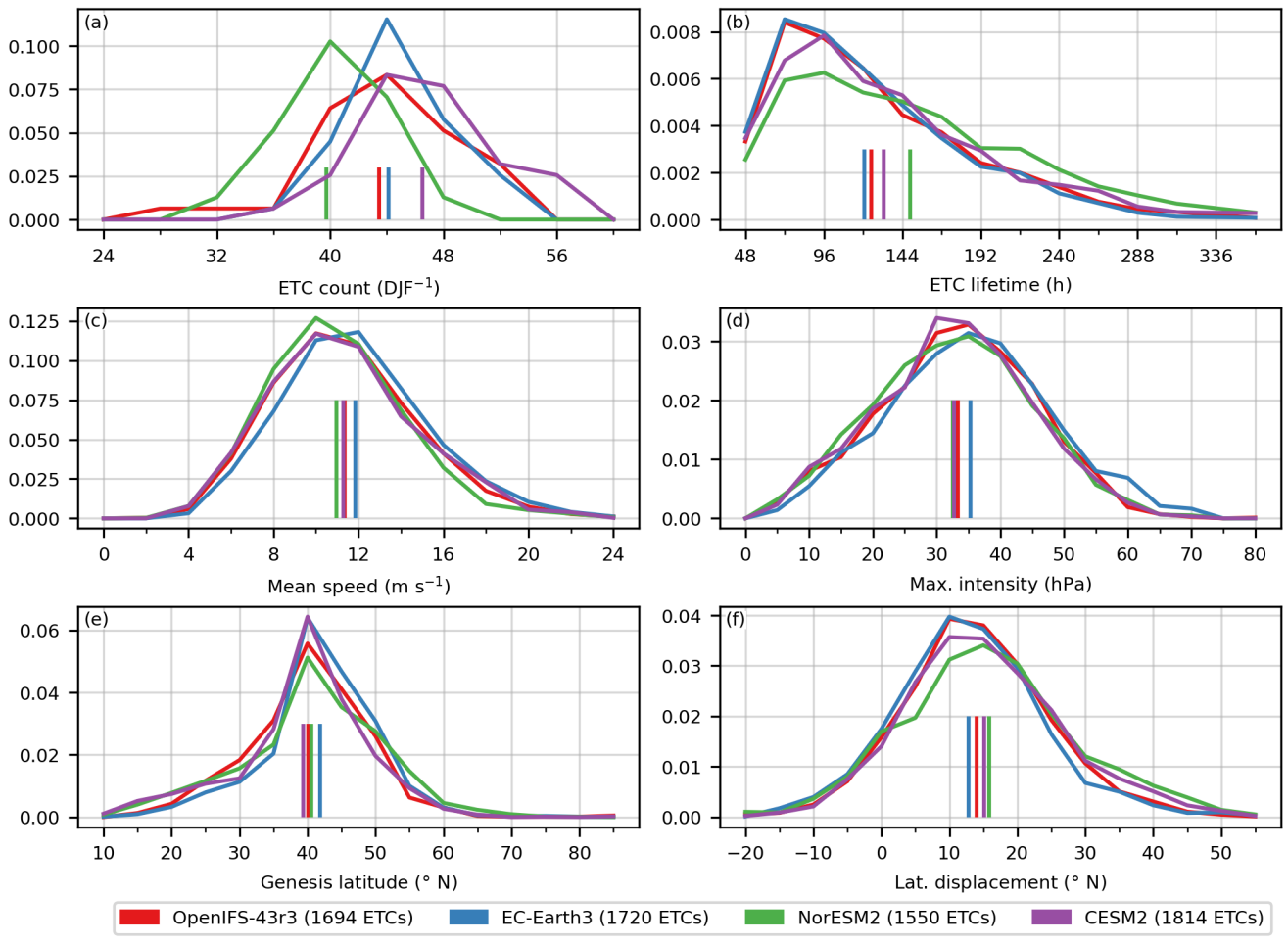

Figure 4. The distribution of six ETC quantities and their mean values shown by vertical lines for the OpenIFS-43r3 (red), EC-Earth3 (blue), NorESM2 (green), and CESM2 (purple). Given in brackets in the legend is the total number of ETCs during 39 DJF periods. The six ETC quantities include ETC count per winter season DJF (a), ETC lifetime (b), mean speed (c), maximum intensity (d), genesis latitude (e), and latitudinal displacement (f). The y-axis gives the probability density. Note that the y-axis are different between panels.

sections in Figure 6, related to the changes in SST. The higher SSTs in the tropics and extratropics lead to a warmer and deeper troposphere. Another common feature across all models is the reduced zonal wind speed u at 250 hPa on the poleward side of the NA jet stream southeast of Greenland.

The most notable and distinguishing aspects across the models are the changes in wind speed in the NA jet stream at the 250 hPa pressure level (Fig. 5). In particular, OpenIFS-43r3 only shows a significant increase on the equatorward side of the jet located over the central Atlantic (Fig. 5a). The remaining three models form a group where the jet speed increases on the jet's southern side and in the jet exit region over Europe. The NorESM2 response presents a single maximum located over the Bay of Biscay with an increase in the zonal wind speed of between 5.0 $\mathrm{m\,s^{-1}}$ and 5.5 $\mathrm{m\,s^{-1}}$ (Fig. 5b). On the other hand, the

https://doi.org/10.5194/egusphere-2024-3713
Preprint. Discussion started: 13 December 2024

CESM2 response (Fig. 5c) shows two maxima, one over the central Atlantic (> 6 $\mathrm{m\ s^{-1}}$) and the other over Europe (5.0 $\mathrm{m\ s^{-1}}$ – 5.5 $\mathrm{m\ s^{-1}}$). Similarly, EC-Earth3 (Fig. 5d) has a similar response to CESM2 with a weaker magnitude at both maxima, 5.0 $\mathrm{m\ s^{-1}}$ – 5.5 $\mathrm{m\ s^{-1}}$ over the central Atlantic and 4.5 $\mathrm{m\ s^{-1}}$ – 5.0 $\mathrm{m\ s^{-1}}$ over Europe.

To gain more insight into the disagreement between OpenIFS-43r3 and the remaining three models, Figure 6 depicts the zonal mean cross-section over Europe (15° W – 35° E), where the responses differ the most. Evidently, the non-existent response in the NA jet exit over Europe in OpenIFS-43r3 is also visible in the cross-section (Fig. 6a). The only statistically significant features are a deceleration of the polar vortex (60° N – 70° N, 150 – 50 hPa) and an upward shift of the subtropical jet stream. The upward shift is present in all models. In contrast, EC-Earth3 responds with a barotropic increase of the NA jet stream between 850 hPa – 350 hPa and 50° N – 60° N (Fig. 6b). Around the jet maximum at 200 hPa, there is a strong vertical shear in ΔFT, suggesting an additional baroclinic contribution. A similar response in the SSP 5-8.5 scenario as EC-Earth3 is found in NorESM2 (Fig. 6c) and CESM2 (Fig. 6d). However, the maximum increase in zonal wind speed u is located equatorward of the NA jet maximum in the respective Baseline simulation. Furthermore, in NorESM2 and CESM2, the response increases in magnitude with height throughout the troposphere (850 hPa – 200 hPa), indicating a more baroclincally-driven response.

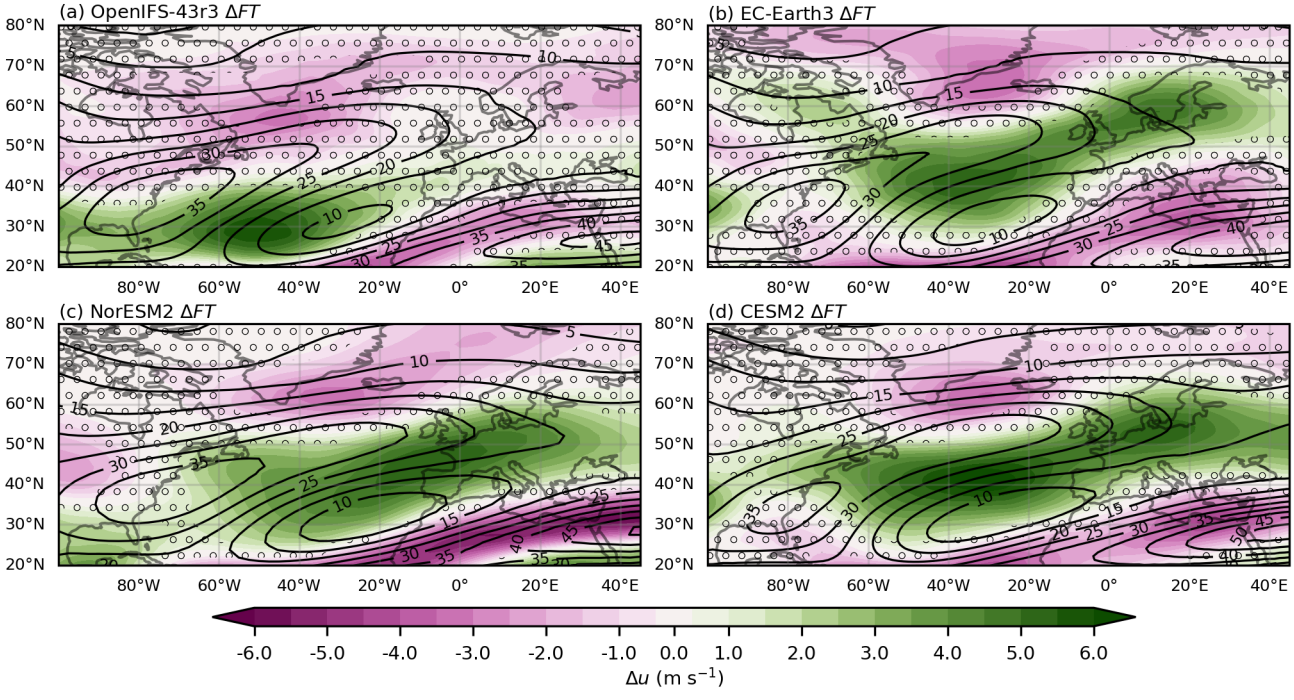

Figure 5. Future response ΔFT in DJF mean of zonal wind speed u at 250 hPa (in colour shading), the Baseline climatology at 250 hPa (in black contours) for (a) OpenIFS-43r3, (b) EC-Earth3, (c) NorEMS2, and (d) CESM2. Stippling indicates statistically insignificant changes (p-value > 0.05).

https://doi.org/10.5194/egusphere-2024-3713
Preprint. Discussion started: 13 December 2024

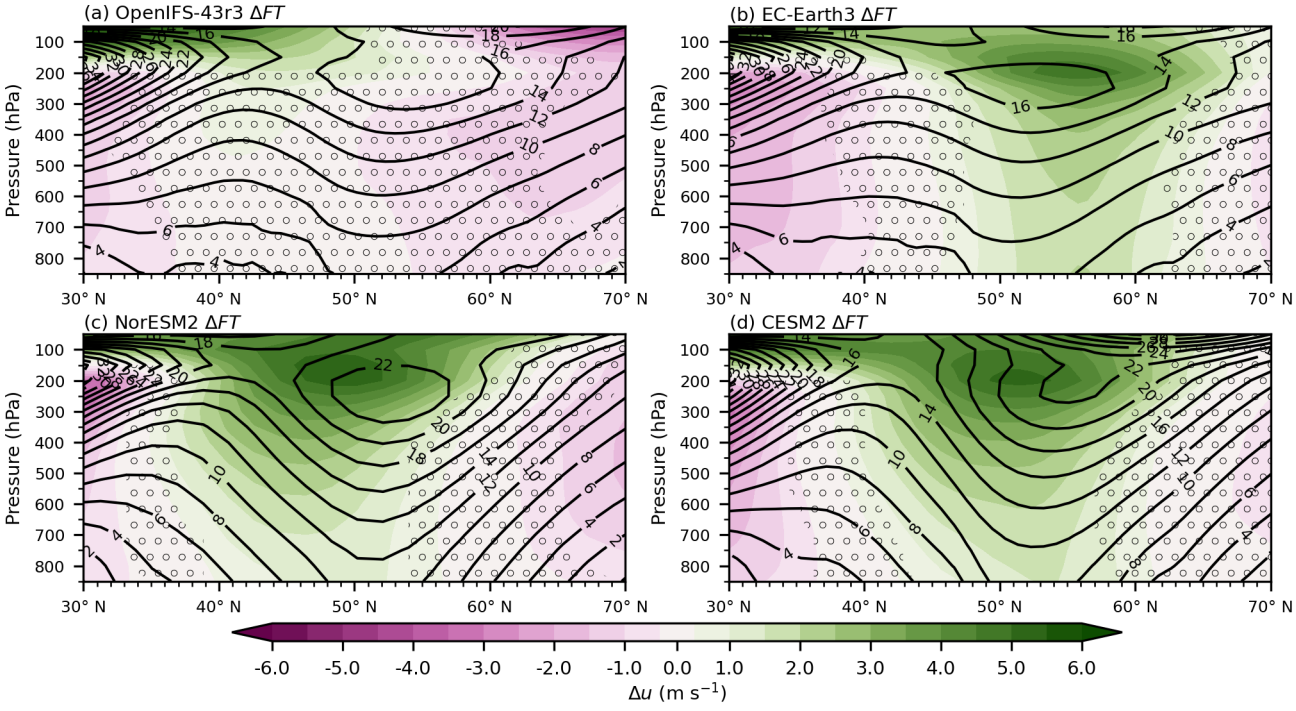

Figure 6. Future response ΔFT of zonal mean (15° W – 35° E) of the 39-year DJF mean of zonal wind speed u (in colour shading), the Baseline climatology (in black contours) for (a) OpenIFS-43r3, (b) EC-Earth3, (c) NorEMS2, and (d) CESM2. Stippling indicates statistically insignificant changes (p-value > 0.05).

4.2 The contribution of SST and SIC

A key goal of the present paper is to investigate the contributions of SST and SIC changes to the combined climate response. The SST response, ΔSST, and SIC response, ΔSIC, of the 250 hPa zonal wind are presented in Figure 7. EC-Earth3, NorESM2, and CESM2 show very similar structures in both contributions. The SST response (Fig. 7c,e,f) closely resembles the Future response (Fig. 5b,c,d), with an increase on the southern side and in the eastern exit region of the NA jet stream. Hence, the future response is largely dominated by changes in SSTs. The SIC response (Fig. 7d,f,h) exhibits a tripole structure. There is a deceleration south of Greenland and around 20° N – 30° N in the Northern Atlantic, and an increase in zonal wind speed at 40° N – 50° N. The exact geographical location and extent of the tripole structure vary between EC-Earth3, NorESM2, and CESM2. Generally, the increases and decreases in SST and SIC response are colocated, resulting in an amplifying effect in the Future response.

OpenIFS-43r3 is the outlier in the SST and SIC response regarding the NA jet stream at 250 hPa. The response to SST in OpenIFS-43r3 (Figure 7a) has broadly the same spatial pattern as in the other models, but it is lower in magnitude. The maximum increase is between 4.0 $\mathrm{m\,s^{-1}}$ and 4.5 $\mathrm{m\,s^{-1}}$, while it exceeds 6.0 $\mathrm{m\,s^{-1}}$ in the other models. However, the key

https://doi.org/10.5194/egusphere-2024-3713
Preprint. Discussion started: 13 December 2024

difference setting OpenIFS-43r3 apart from the other models is identifiable in the SIC response (Fig. 7b). In OpenIFS-43r3, there is an absence of a tripole structure and a significant decrease relative to the Baseline simulation in the wind speed in the NA jet exit region over Europe. The SST-related increase and SIC-related decrease over Europe compensate each other, resulting in the lack of the response in ΔFT (Fig. 5a).

The cross-section of the zonal wind speed u and its response to changed SSTs from the OpenIFS-43r3 simulations are shown in Figure 8a. This reaffirms the compensating contributions of changed SSTs and SIC. Due to increased SSTs, the subtropical jet shifts upwards and the NA jet stream increases in speed between 300 hPa and 100 hPa. Meanwhile, the SIC response shows a reduction in the NA jet speed throughout the troposphere (Fig. 8b). The change in SIC is also the origin of the deceleration of the polar vortex in the Future response (Fig. 8a).

EC-Earth3 shows no significant response in the jet stream due to changes in SIC in the zonal mean cross-section over Europe (Fig. 8d). These weak non-significant changes overlap with the SST response in Figure 8c. The SST response shows strong similarities with the Future response (Fig. 6b).

NorESM2 and CESM2 present structurally similar SST responses and SIC responses for the zonal wind speed u. The SST responses (Fig. 8e,g) show an intensification of the NA jet stream equatorward of jet core in the Baseline simulation. Both models exhibit a response in the zonal wind speed, which has a vertical gradient between 850 hPa and 200 hPa, with the strongest response at upper levels. However, in CESM2 the response is stronger (5.5 $\mathrm{m\,s^{-1}}$ – 6.0 $\mathrm{m\,s^{-1}}$) compared to NorESM2's peak response which lies between 5.0 $\mathrm{m\,s^{-1}}$ and 5.5 $\mathrm{m\,s^{-1}}$. For NorESM2 and CESM2, the SIC response (Fig. 8f,h) is characterised by a dipole feature with a reduction on the poleward side and an increase on the equatorward side. The dipole has a weak vertical gradient. The dipole structure is a statistically significant feature in NorESM2, but not in CESM2.

5 The mechanisms of the jet response

This section explains the SST and SIC response in zonal wind speed u with the aid of the response in the meridional baroclinicity B_y and momentum flux convergence MFC. In the following, the SST response across all models is presented first due to its dominating role in the Future zonal wind speed response.

5.1 The mechanisms for SST response

A feature common to all models is the impact of SSTs on baroclinicity B_y driving the change of the subtropical jet (Fig. 9a,c,e,g, 30° N – 35° N). The baroclinicity between 850 hPa and 300 hPa decreases, while an increase is visible from 300 hPa to 100 hPa. This corresponds well with the upward shift of the subtropical jet described in Section 4.2. The origin of the increased baroclinicity above 300 hPa is an increased upper-level warming in the tropics (not shown) and an upper-level cooling in the potential temperature in the subtropics/midlatitudes (Fig. 10a,c,e,g, 30° N – 35° N, 200 hPa – 100 hPa). The deepening of the troposphere due to warming SSTs and the subsequent lifting of the thermal tropopause explains the cooling. The tropospheric deepening, and subsequent increase in jet height, also explains the increase in momentum flux convergence

https://doi.org/10.5194/egusphere-2024-3713
Preprint. Discussion started: 13 December 2024

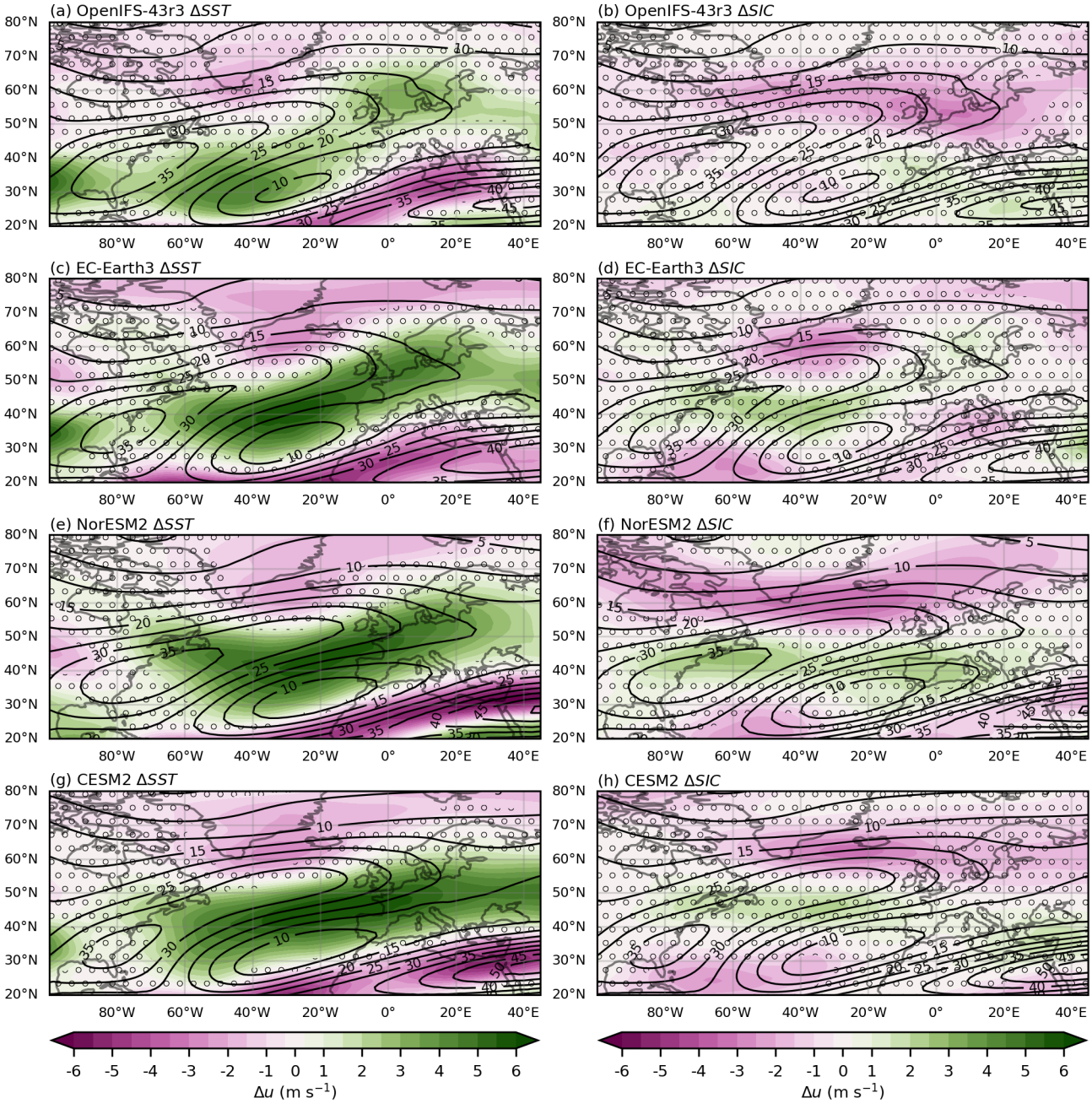

Figure 7. SST response ΔSST (a,c,e,g) and SIC response ΔSIC (b,d,f,h) of DJF mean of zonal wind speed u at 250 hPa (in colour shading), the Baseline climatology at 250 hPa (in black contours) for (a) & (b) OpenIFS-43r3, (c) & (d) EC-Earth3, (e) & (f) NorEMS2, and (g) & (h) CESM2. Stippling indicates statistically insignificant changes (p-value > 0.05).

https://doi.org/10.5194/egusphere-2024-3713
Preprint. Discussion started: 13 December 2024

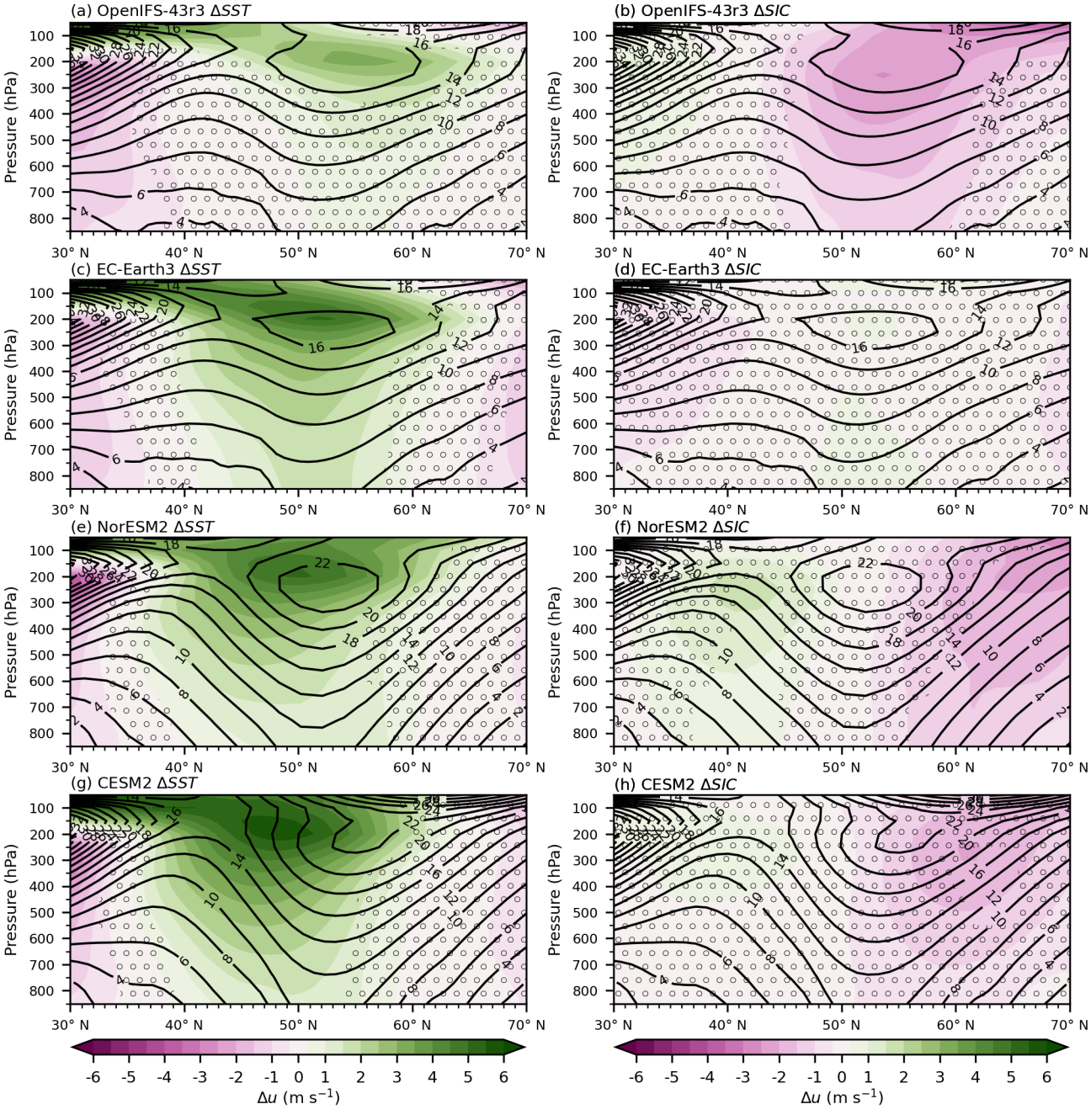

Figure 8. SST response ΔSST (a,c,e,g) and SIC response ΔSIC (b,d,f,h) of the zonal mean (15° W – 35° E) of the 39-year DJF mean of zonal wind speed u (in colour shading), the Baseline climatology (in black contours) for (a) & (b) OpenIFS-43r3, (c) & (d) EC-Earth3, (e) & (f) NorEMS2, and (g) & (h) CESM2. Stippling indicates statistically insignificant changes (p-value > 0.05).

https://doi.org/10.5194/egusphere-2024-3713
Preprint. Discussion started: 13 December 2024

MFC located above the maxima in the respective Baseline simulation for all models (Fig. 11a,c,e,g, 40° N – 60° N, 300 hPa – 100 hPa).

In OpenIFS-43r3 (Fig. 9a), the baroclinicity associated with the NA jet exit (45° N – 65° N) increases at upper levels (400 hPa – 200 hPa); this results in the shallow response of the zonal wind speed seen in Figure 8a. The increase in baroclinicity is caused by a larger increase in potential temperature at lower latitudes (30° N – 50° N) compared to higher latitudes (50° N – 70° N). This meridional difference in potential temperature increase is the strongest between 400 hPa – 300 hPa (Fig. 10a). The momentum flux convergence in OpenIFS-43r3, MFC, increases at the location of the zonal wind speed increase (45° N – 65° N, 200 hPa – 100 hPa). Like the zonal wind speed response, OpenIFS-43r3 shows the weakest response in MFC among all models.

EC-Earth3 shows a very similar SST response to OpenIFS-43r3 with two distinct differences (Fig. 9c). First, the upper-level baroclinicity increase (45° N – 65° N, 400 hPa – 200 hPa) is stronger, exceeding $6.0{\cdot}10^{-4}$ s^{-1}. This is the consequence of a stronger upper-level warming in EC-Earth3 (Fig. 10c, 30° N – 40° N, 400 hPa – 200 hPa). Furthermore, the enhanced baroclinicity response explains the stronger increase in the upper-level part of the NA jet stream exit in EC-Earth3 compared to OpenIFS-43r3, as shown in Section 4.2. Second in EC-Earth3, there is a weak increase in baroclinicity from 40° N to 50° N and between 700 hPa and 400 hPa, which results from a more pronounced warming at the subtropical middle troposphere (30° N – 40° N, 400 hPa – 700 hPa). However, this increase in baroclinicity does not explain the increase in zonal wind speed u at lower levels (500 hPa – 850 hPa) in Figure 8c, as the maximum is located between 49° N – 54° N. This requires the momentum flux convergence MFC (Fig. 11c), which shows an increase at the lower levels in EC-Earth3 (47° N – 53° N, 500 hPa – 850 hPa). An increase in MFC leads to a barotropic increase in zonal wind speed, present in Figure 8c. Furthermore, there is a decrease in momentum flux convergence MFC between 60° N and 70° N at upper levels (400 hPa – 200 hPa), which is co-located with an increase in baroclinicity. These effects are compensating, resulting in a reduced increase in zonal wind speed co-located with a MFC decrease.

The SST response of baroclinicity in NorESM2 (Fig. 9e) is structurally similar to EC-Earth3. The strongest increases in baroclinicity are found at 400 hPa to 200 hPa and from 40° N to 60° N, the peak value exceeding $6.0{\cdot}10^{-4}$ s^{-1}. Additionally, NorESM2 also features a weak but significant increase in baroclinicity at lower levels (500 hPa – 850 hPa, 35° N – 50° N), which is more pronounced relative to EC-Earth3. Contrary to EC-Earth3, the origin of the baroclinicity response in NorESM2 is slightly different. Figure 10e shows that the upper-level warming between 30° N and 45° N is weaker in NorESM2 compared to EC-Earth3. Likewise, the upper-level potential temperature increase at latitudes 45° N to 70° N is weaker, resulting in a comparable baroclinicity response. NorESM2, like the other models, shows the strongest increase in momentum flux convergence co-located with the zonal wind speed increase (Fig. 11e). Moreover, like EC-Earth3, NorESM2 exhibits the compensating effect of baroclinicity and MFC, found at 60° N to 70° N and 400 hPa to 200 hPa, resulting in a non-significant change in zonal wind speed (Fig. 8e).

Lastly, CESM2 shows a baroclinicity response structurally similar to NorESM2, but with an amplified magnitude (Fig. 9g). This results from weaker warming of the atmospheric column at higher latitudes (55° N – 70° N) in CESM2 compared to NorESM2, while the warming at lower latitudes (30° N – 55° N) is comparable (Fig. 10g). Like the other models, the change

https://doi.org/10.5194/egusphere-2024-3713
Preprint. Discussion started: 13 December 2024

in baroclinicity and MFC act together to increase the jet speed located above the maximum in the Baseline simulation. Nonetheless, the momentum flux convergence MFC contributes a weak amplification of the zonal wind speed at lower levels (850 hPa – 600 hPa, 52° N – 58° N) in Figure 11g.

5.2 The mechanisms for SIC response

OpenIFS-43r3 shows the geographically most extensive reduction in baroclinicity B_y across all models (Fig. 9b). The decrease exceeding the magnitude of $1.2{\cdot}10^{-4}$ s^{-1} reaches from 47° N to 70° N and is vertically deep from 850 hPa to 300 hPa. The baroclinicity response originates from deep vertical warming at 60° N to 70° N (Fig. 10b) with the strongest warming located at the surface. This warming is directly induced by sea ice removal, exposing the sea surface to the atmosphere. A secondary effect is a cooling at lower latitudes (35° N – 50° N), which has its maximum at 500 hPa to 300 hPa. This dipole structure has been identified in previous studies (Screen et al., 2022; Labe et al., 2020). Furthermore, the momentum flux convergence shows a non-significant reduction colocated with its Baseline maximum (Fig. 11b, 50° N – 60° N, 400 hPa – 200 hPa). The baroclinicity change is the primary driver of the zonal wind speed response, as previously discussed.

The SIC response of zonal wind speed in EC-Earth3 does not show any significant changes. This is the result of opposing effects of momentum flux convergence MFC and baroclinicity B_y. The MFC shows a dipole structure (Fig. 11d), where there is an increase at the location of the Baseline maximum and a decrease poleward of it. Meanwhile, the EC-Earth3 baroclinicity shows the weakest SIC response of all models (Fig. 9d). Relevant to the NA jet stream exit is the reduction found at 50° N to 60° N and 850 hPa to 500 hPa, which implies a decrease in zonal wind speed but is offset by the MFC increase. Moreover, the MFC decrease is offset by an increase in baroclinicity at 65° N to 70° N and 500 hPa to 300 hPa.

The dominating factor in NorESM2 is the momentum flux convergence MFC (Fig. 11f). There is a dipole with an increase on the equatorward side and a decrease on the poleward side of the Baseline maximum. This results in the equatorward shift of the NA jet stream exit in NorESM2. Supporting the equatorward shift in zonal wind speed is a decrease in baroclinicity on the poleward side (60° N – 70° N, 850 hPa – 700 hPa) and an increase on the equatorward side (40° N – 50° N, 500 hPa – 300 hPa), shown in Figure 9f. The cause of the reduction in baroclinicity B_y is shallow warming at high latitudes (60° N – 70° N, 850 hPa – 700 hPa) resulting directly from the removal of sea ice (Fig. 10f). Additionally, the increase in B_y results from a warming at 30° N to 40° N and a cooling at 50° N to 65° N.

CESM2 responds to the decreased SIC with a vertically extensive reduction in baroclinicity reaching from 850 hPa to 400 hPa located between 53° N and 70° N (Fig. 9h). This reduction originates similarly to OpenIFS-43r3 from deep high-latitude vertical warming (60° N – 70° N, 850 hPa – 400 hPa) and an adjacent cooling equatorward of the warming (Fig. 10h). The momentum flux convergence MFC presents a dipole structure, which is not associated with a corresponding dipole in the zonal wind speed. This indicates that the baroclinicity change is the dominating factor for the SIC response in CESM2.

https://doi.org/10.5194/egusphere-2024-3713
Preprint. Discussion started: 13 December 2024

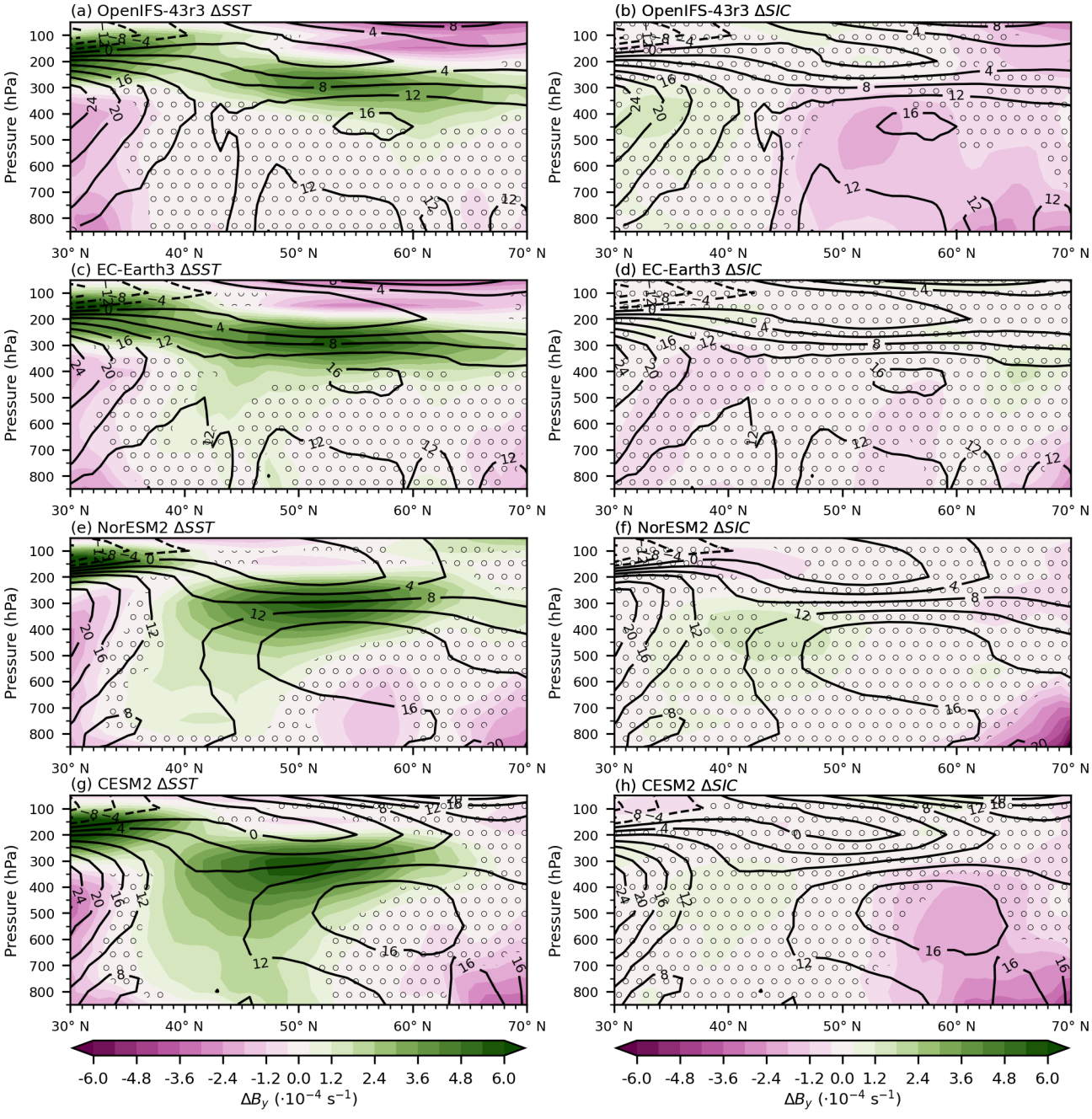

Figure 9. SST response ΔSST (a,c,e,g) and SIC response ΔSIC (b,d,f,h) of the zonal mean (15° W – 35° E) of the 39-year DJF mean of baroclinicity B_y (in colour shading), the Baseline climatology (in black contours) for (a) & (b) OpenIFS-43r3, (c) & (d) EC-Earth3, (e) & (f) NorEMS2, and (g) & (h) CESM2. Stippling indicates statistically insignificant changes (p-value > 0.05).

https://doi.org/10.5194/egusphere-2024-3713
Preprint. Discussion started: 13 December 2024

6 The extra-tropical cyclone response

This section addresses the Future, SST, and SIC responses of ETC track densities and the six previously introduced ETC properties, related to the changes in the North Atlantic jet stream.

6.1 The Future response of ETC track density

Figure 12 shows the Future response of the ETC densities for all four models. In OpenIFS-43r3, the majority of the ETC track density changes compared to the Baseline simulation are non-significant. Significant reductions are, however, present in the location of the storm track maxima over the Eastern US and Western Atlantic. Furthermore, Europe (30° N – 70° N, 15° W – 35° E) sees a non-significant reduction in ETC track density.

Next, in EC-Earth3, the Future response shows a clearer signal (Fig. 12b). There is an increase in ETC track density exceeding 4 ETCs per 5° spherical cap per winter season downstream of the Baseline storm track. This increase is tied to the eastward extension of the NA jet stream. Specifically, the ETC track density is increased northward of the zonal wind speed increase. Additionally, there is a significant decrease east of Greenland and over the European continent.

NorESM2 is set apart by a significant decrease in ETC track density in the storm track in the Future simulation (Fig. 12c). The maximum decrease is found around Iceland with a magnitude > 12 ETCs per 5° spherical cap per winter season. Furthermore, the ETC track density in the Mediterranean is reduced by 2 ETCs per 5° spherical cap per winter season. Similarly to EC-Earth3, the increase in ETC track density over Northern Europe is tied to the increase in the NA jet stream.

CESM2 presents an increase downstream of the Baseline storm tracks (Fig. 12d). As with other models, this is co-located with the increase of the Future response of the NA jet stream. Also, CESM2 show its strongest reduction in ETC track density eastward of Greenland, and the Western Atlantic. Over the Mediterranean, there is a relatively weaker, nonetheless significant, decrease in the ETC track density.

6.2 The SST and SIC contributions

Due to the sparser nature and higher variability of the ETC dataset compared to, for example, the zonal wind speed, the contribution of SSTs and SIC do not sum up to the Future response, resulting in a larger residual, as discussed in Section 2.5. Nonetheless, it is useful to look at the effects of changed SST and SIC individually.

OpenIFS-43r3 shows a reduction of ETC track density over the Eastern US and Western Atlantic as a response to increased SSTs. (Fig. 13a). There is an increase in ETC in the Eastern Atlantic (48° N – 60° N, 40° W – 5° W), extending the storm track to the east. This eastward extension is located north of the zonal wind increase (Fig. 7a). Meanwhile, in the SIC response (Fig. 13b), a clear feature is a dipole southeast of Greenland, effectively leading the southward shift. In the Mediterranean, the SST and SIC responses are opposed to each other with ΔSST showing a decrease in ETC track density and ΔSIC showing an increase.

EC-Earth3's SST response is characterised by a shift of the storm track towards the southeast (Fig. 13c). The strongest decrease takes place between Greenland and Iceland. Moreover, there is a significant decrease in the Mediterranean area and

https://doi.org/10.5194/egusphere-2024-3713
Preprint. Discussion started: 13 December 2024

the Arctic Ocean. Meanwhile, there is an extensive increase in ETC track density over the Eastern Atlantic Ocean (40° N – 58° N, 40° W – 5° E). The SIC response presents a similar dipole (Fig. 13d), with a reduction southeast of Greenland and an increase over the central Atlantic (40° N – 58° N, 50° W – 20° W). The compounding effects of the SST and SIC response explain the clearer increase over Northern Europe and decrease over Central Europe in the Future response in EC-Earth3. Both SST and SIC responses show a strong connection with the jet stream changes (Fig. 7c,d). The widespread increases in ETC track density are located northward of the increase in jet speed.

For NorESM2, the SST response (Fig. 13e) majorly contributes to the reduction in ETC track density in the Future response. This reduction is primarily located in the storm track from the Eastern US along the Western Atlantic towards Greenland. Additionally, the change in SST is the origin of the decrease in the Mediterranean. While NorESM2 shows a similarly strong increase in zonal wind speed in the SST response as EC-Earth3, NorESM2 shows a weaker positive response in the ETC track density compared to EC-Earth3. Meanwhile, the change in SIC (Fig. 13f) is responsible for the reduction located over Iceland and the Arctic Ocean. SSTs and SIC contribute to an increase over Northern Europe and the British Isles, with the SIC response having a larger magnitude (8 to 9 ETCs per 5° spherical cap per winter season).

In CESM2, similar to NorESM2, the changed SSTs reduce the ETC track density along the Baseline simulation storm track and the Mediterranean (Fig. 13g). However, the reduction in the Arctic Ocean due to SST changes is more pronounced in CESM2. The increases in ETC track density in the North Atlantic are statistically insignificant, and like the other models, they are located northward of the increases in the zonal wind. The SIC response has the largest impact in the Arctic Ocean (Fig. 13h, 60° N – 80° N, 25° W – 20° E). The Future response of CESM2 shows a clearer signal compared to the individual contributions of SST and SIC. However, the individual contributions have similar spatial patterns, indicating that the Future response in CESM2 is not dominated by either SST or SIC.

6.3 The impacts on ETC properties

Figure 14 presents the changes in the mean value of ETC count, ETC lifetime, mean speed, maximum intensity, genesis latitude, and latitudinal displacement for ETCs affecting Europe (30° N – 70° N, 15° W – 35° E). Similar to the track densities, the SIC response ΔSIC and SST response ΔSST do not necessarily add linearly to exactly equal the Future response. However, they provide insight into the dominating contribution to the Future response and help to compare the responses across models. The diamonds in Figure 14 represent the mean value of the ETC properties in the Baseline simulation, which has been previously discussed in Section 3.3 (Figure 4). The inclusion of the Baseline simulation sets the responses of each model in the context of model differences. Considering ETC properties, the majority of Future, SIC and SST responses are smaller than the differences between the individual models. In particular, ETC count and genesis latitude are properties which show responses of a magnitude similar to the model differences.

The ETC count per winter season DJF shows a decrease in the Future response originating from the SST response (Fig. 14a) across models, with the change being statistically significant in NorESM2 (ΔFT, -2.3 DJF^{-1}) and CESM2 (ΔFT, -4.5 DJF^{-1}). Models disagree on the effect of changed SIC on ETC count. OpenIFS-43r3 is the only model with a significant

https://doi.org/10.5194/egusphere-2024-3713
Preprint. Discussion started: 13 December 2024

change by +2.4 per winter season DJF, which is corresponds to the increase in ETC track density found in the Mediterranean (Fig. 13b).

The SIC and SST response of ETC lifetime contribute similarly in magnitude to the Future response (Fig. 14b). EC-Earth3 and CESM2 present an increase in lifetime for ΔSST and ΔSIC, which results in a significant increase in the Future response (EC-Earth3: +5.0 h, CESM2: +7.5 h). Meanwhile, OpenIFS-43r3 shows a non-significant decrease in ETC lifetime for ΔSST and a non-significant increase for ΔSIC, which compensate each other in the Future response. There are only minimal, non-significant changes to the ETC lifetime in NorESM2. The mean speed of ETCs does not show any significant changes (Fig. 14c), besides a deceleration in EC-Earth3's Future response (-0.27 $\mathrm{m\,s^{-1}}$). Additionally, the models disagree on the sign of the change for the Future, SST and SIC response.

For the mean maximum intensity (quantified by the magnitude of the pressure anomaly), models agree on an increase in response to the SST changes, indicating a deepening of ETCs, and a decrease in response to the SIC changes, corresponding to a reduction of the pressure minimum (Fig. 14d). However, many of these changes are not significant. NorESM2 shows a significant decrease due to SIC changes (-1.8 hPa) and a minimal non-significant change due to ΔSST, which results in a reduced maximum intensity on average in the Future response. Next, while EC-Earth3 presents a significant increase in maximum intensity for ΔSST, the Future response, like the SIC response, shows a non-significant decrease.

The Future response of the genesis latitude is dominated by the change in SSTs with a significant increase across all models (Fig. 14e). Averaged across models, the genesis latitude increases by +1.1° N in ΔFT and +1.3° N in ΔSST. The SIC responses are non-significant across models. Figure 14f shows the latitudinal displacement of ETCs which is significantly reduced in OpenIFS-43r3 and NorESM2 for the Future response. For NorESM2, the change originates from the SST change and the interaction of the SST and SIC changes. Meanwhile, the SIC response dominates for OpenIFS-43r3. The SST responses are not significant in any of the four models. Combining the changes in the genesis latitude and latitudinal displacement ETCs are propagating further north in the SST change only simulation. However, in the Future climate scenario ETCs travel more zonally in OpenIFS-43r3, EC-Earth3, NorESM2, which indicates important interactions of SST and SIC changes.

7 Conclusions

This study presents the responses of the North Atlantic jet stream and storm track to future sea surface temperatures and sea ice cover and quantifies their contributions using the set of atmosphere-only model simulations from the CRiceS project (CRiceS). Furthermore, the potential driving mechanism of the responses were examined by using the baroclinicity and momentum flux convergence. The key findings of this study are as follows:

- The Baseline simulations of the four models agree on the general shape of the North Atlantic jet stream and baroclinicity. A key difference is that the zonal wind speed u in the upper troposphere is higher over Europe in NorESM2 and CESM2 compared to EC-Earth3 and OpenIFS-43r3. The difference in the jet strength over Europe is primarily explained by the magnitude of momentum flux convergence in the Baseline simulation. The ETC track density is similar across models, with EC-Earth3 and OpenIFS-43r3 exhibiting lower values east of North America and Greenland than NorESM2 and

https://doi.org/10.5194/egusphere-2024-3713
Preprint. Discussion started: 13 December 2024

CESM2. The patterns of the ETC track density and NA jet stream in the Baseline simulation closely match previous findings based on the ERA5 reanalysis and CMIP6 simulations (Harvey et al., 2020; Priestley et al., 2020), as well as the PAMIP intercomparison (Yu et al., 2023). Thus, it is concluded that the model simulations used here are appropriate for studying future changes.

- In the Future response, three out of the four models show an increase in zonal wind speed at 250 hPa on the southeastern side of the Baseline jet core over the eastern North Atlantic and reaching far into Europe, which has been shown in CMIP6 simulations (Harvey et al., 2020). The ΔSST contribution dominates the Future response by an increase in the upper tropospheric baroclinicity. The momentum flux convergence contributes to an equatorward shift of the NA jet stream in the SIC response.

- The exception is OpenIFS-43r3 with no significant change in zonal wind speed over Europe. The SST response is similar to the other three models, meanwhile, the SIC response shows a decrease in zonal wind speed over Europe, which is driven by a decrease by more than 10 % in baroclinicity at lower levels (850 hPa – 400 hPa). These opposite responses result in no significant changes to the jet stream over Europe in the Future scenario.

- The ETC track density reduces along the East coast of Northern America and Greenland in the Future scenario. SST and SIC effects both significantly contribute to the reduction. The increases in ETC track density over the Eastern North Atlantic, leading to an eastward extension of the storm track, are associated with the extension of the NA jet stream. Similar to the jet stream changes, OpenIFS-43r3 shows no significant increases over Europe in the ETC track density in the Future. The eastward extension of the storm track has been shown in CMIP6 (Priestley and Catto, 2022; Harvey et al., 2020), where SST and SIC are changing, and PAMIP simulations with changed SIC only (Hay et al., 2023). Across all models, a consistent feature is a significant reduction of ETC track density in the Mediterranean basin, which are driven by the changes in SSTs. The reduction in the Mediterranean basin is also present in CMIP projections (Priestley and Catto, 2022).

- The future changes to the mean values of the ETC-specific properties are superseded by the inter-model differences. For example, mean speed and maximum intensity show no consistent statistically significant changes for 2 or more models. However, ETC affecting Europe tend to become less frequent, which is linked to the reduced ETC track density in the Mediterranean, and originate more poleward in the Future scenario, which is driven by changes in SSTs.

- It has been shown that the total future response of the North Atlantic at 250 hPa is dominated by the changes in sea surface temperature. On the other hand, the contributions of changes in sea ice cover and sea surface temperature to the total future response of the North Atlantic storm track are of similar magnitude.

This study is based on atmosphere-only simulations with annually repeating sea-ice cover and sea surface temperatures, which limits the comparability between the studied simulations and results from reanalysis and CMIP. Furthermore, the changes presented are the mean responses of the jet stream and storm track, leaving the investigation of changes to the variability and

https://doi.org/10.5194/egusphere-2024-3713
Preprint. Discussion started: 13 December 2024

extreme events of the jet stream and storm track to future research. Moreover, one aim of the coordinated simulations is to constrain the variability of the climate system. However, the internal atmospheric climate variability is a major source of uncertainty in this study. This affects both the study between the differences between simulations within one model and the comparison between the four different models. In particular, the metrics related to extratropical cyclones are strongly affected by atmospheric internal variability. In addition, motivated by the model-specific physical interpretability, the model number is limited. Thus, it is difficult to assess whether the disagreement of OpenIFS-43r3 response is an outlier or a representative of a different part of spread of state-of-the-art models.

Notable differences in the Future responses occur, despite the models having similar Baseline climates, and being forced with the same changes to SSTs and sea-ice cover. Furthermore, although the SST response dominates, the sea ice cover (SIC) response is significant in some areas. For example, in OpenIFS-43r3 the SIC response is large enough to counteract the impact of changing SSTs. Overall, substantial uncertainties remain in how the jet stream and storm track in the Northern Atlantic and Europe will change in the future.

Code and data availability. The cyclone tracking algorithm TRACK is available on GitHub (Hodges, 2020). The data and scripts necessary to produce the plots are available on Zenodo (Köhler et al., 2024).

The full CRiceS simulation data set is available as follows:

OpenIFS-43r3: https://a3s.fi/CRiceS_Index/CRiceS_index.html. EC-Earth3: https://crices-task33-output-ecearth.lake.fmi.fi/index.html and https://crices-task33-output-ecearth-ifs-monthly-means.lake.fmi.fi/index.html. NorESM2: At the moment NorESM2 data is available from authors upon request and it will be published to a public archive during the review process. CESM2: https://archive.sigma2.no/pages/public/datasetDetail.jsf?id=10.11582/2024.00018.

The model code is available as follows:

OpenIFS-43r3: Documentation is available at https://confluence.ecmwf.int/display/OIFS. The licence for using the OpenIFS model can be requested from ECMWF user support (openifs-support@ecmwf.int). EC-Earth3: Brief general documentation of EC-Earth3 is provided at https://ec-earth.org/ec-earth/ec-earth3/. The code is available to registered users at https://ec-earth.org/ec-earth/ec-earth-development-portal/. Only employees of institutes that are part of the EC-Earth consortium can obtain an account. NorESM2: Documentation is available at https://www.noresm.org/. The code is available at https://github.com/NorESMhub/NorESM. CESM2: documentation is available at https://escomp.github.io/CESM/versions/cesm2.2/html/. The code is available at: https://github.com/ESCOMP/CESM.

Appendix A

Author contributions. DK and VS contributed to the design of the study. DK performed the analysis with guidance from VS. DK wrote the publication, supported by VS, PR, TN, and KN. The model simulations have been conducted by DK (OpenIFS-43r3), PR (EC-Earth3), TN (NorESM2), KN (CESM2).

https://doi.org/10.5194/egusphere-2024-3713
Preprint. Discussion started: 13 December 2024

ETC count (DJF^{-1})	OpenIFS-43r3	EC-Earth3	NorESM2	CESM2	Track duration (h)	OpenIFS-43r3	EC-Earth3	NorESM2	CESM2
OpenIFS-43r3	(43.436)	-0.667	**3.692**	**-3.077**	OpenIFS-43r3	(124.867)	**4.249**	**-23.910**	**-7.620**
EC-Earth3	0.667	(44.103)	**4.359**	**-2.410**	EC-Earth3	**-4.249**	(120.617)	**-28.159**	**-11.869**
NorESM2	**-3.692**	**-4.359**	(39.744)	**-6.769**	NorESM2	**23.910**	**28.159**	(148.777)	**16.291**
CESM2	**3.077**	**2.410**	**6.769**	(46.512)	CESM2	**7.620**	**11.869**	**-16.291**	(132.486)
Mean speed (m s^{-1})	OpenIFS-43r3	EC-Earth3	NorESM2	CESM2	Max. intensity (hPa)	OpenIFS-43r3	EC-Earth3	NorESM2	CESM2
OpenIFS-43r3	(11.343)	**-0.509**	**0.370**	0.071	OpenIFS-43r3	(33.291)	**-2.029**	0.764	0.540
EC-Earth3	**0.509**	(11.852)	**0.879**	**0.580**	EC-Earth3	**2.029**	(35.320)	**2.793**	**2.569**
NorESM2	**-0.370**	**-0.879**	(10.972)	**-0.299**	NorESM2	-0.764	**-2.793**	(32.527)	-0.224
CESM2	-0.071	**-0.580**	**0.299**	(11.271)	CESM2	-0.540	**-2.569**	0.224	(32.750)
Lat. of gen. (° N)	OpenIFS-43r3	EC-Earth3	NorESM2	CESM2	Lat. displ. (° N)	OpenIFS-43r3	EC-Earth3	NorESM2	CESM2
OpenIFS-43r3	(40.130)	**-1.702**	-0.471	**0.779**	OpenIFS-43r3	(13.971)	**1.182**	**-1.872**	**-1.149**
EC-Earth3	**1.702**	(41.832)	**1.231**	**2.481**	EC-Earth3	**-1.182**	(12.789)	**-3.054**	**-2.331**
NorESM2	0.471	**-1.231**	(40.601)	**1.250**	NorESM2	**1.872**	**3.054**	(15.843)	**0.723**
CESM2	**-0.779**	**-2.481**	**-1.250**	(39.351)	CESM2	**1.149**	**2.331**	**-0.723**	(15.120)

Table A1. Additional information to Figure 4. For the six ETC quantities, the mean value for each model is reported on the diagonal (in parentheses) and the differences between the models (row - column) are given in the off-diagonal cells. A t-test p-value < 0.05 is highlighted in bold font.

Competing interests. The authors declare that they have no conflict of interest.

Acknowledgements. This project has received funding from the European Union's Horizon 2020 research and innovation programme under grant agreement No 101003826 via project CRiceS (Climate Relevant interactions and feedbacks: the key role of sea ice and Snow in the polar and global climate system). This research was also supported by the Academy of Finland (grant no. 338615). We wish to thank Kevin Hodges for providing the cyclone tracking software TRACK. We acknowledge CSC – IT Centre for Science, Finland, for providing generous computational resources.

https://doi.org/10.5194/egusphere-2024-3713
Preprint. Discussion started: 13 December 2024

References

Athanasiadis, P. J., Wallace, J. M., and Wettstein, J. J.: Patterns of Wintertime Jet Stream Variability and Their Relation to the Storm Tracks, J. Atmos. Sci., 67, 1361–1381, https://doi.org/10.1175/2009JAS3270.1, 2010.

Barnes, E. A. and Screen, J. A.: The impact of Arctic warming on the midlatitude jet-stream: Can it? Has it? Will it?, WIREs Climate Change, 6, 277–286, https://doi.org/10.1002/wcc.337, 2015.

Cai, M. and Mak, M.: Symbiotic Relation between Planetary and Synoptic-Scale Waves, J. Atmos. Sci., 47, 2953–2968, https://doi.org/10.1175/1520-0469(1990)047<2953:SRBPAS>2.0.CO;2, 1990.

Chemke, R., Polvani, L. M., and Deser, C.: The Effect of Arctic Sea Ice Loss on the Hadley Circulation, Geophys. Res. Lett., 46, 963–972, https://doi.org/10.1029/2018GL081110, 2019.

CRiceS: Climate Relevant interactions and feedbacks: the key role of sea ice and Snow in the polar and global climate system, https://www.crices-h2020.eu, (last access: 27 November 2024), 2021.

Dai, A. and Song, M.: Little influence of Arctic amplification on mid-latitude climate, Nature Climate Change, 10, 231–237, https://doi.org/10.1038/s41558-020-0694-3, 2020.

Eliassen, A. and Palm, E.: On the transfer of energy in stationary mountain waves., Geofys. Publ., 22, 1–23, 1961.

Eyring, V., Bony, S., Meehl, G. A., Senior, C. A., Stevens, B., Stouffer, R. J., and Taylor, K. E.: Overview of the Coupled Model Intercomparison Project Phase 6 (CMIP6) experimental design and organization, Geoscientific Model Development, 9, 1937–1958, https://doi.org/10.5194/gmd-9-1937-2016, 2016.

Gramcianinov, C. B., Campos, R. M., de Camargo, R., Hodges, K. I., Guedes Soares, C., and da Silva Dias, P. L.: Analysis of Atlantic extratropical storm tracks characteristics in 41 years of ERA5 and CFSR/CFSv2 databases, Ocean Engineering, 216, 108 111, https://doi.org/10.1016/j.oceaneng.2020.108111, 2020.

Harvey, B. J., Cook, P., Shaffrey, L. C., and Schiemann, R.: The Response of the Northern Hemisphere Storm Tracks and Jet Streams to Climate Change in the CMIP3, CMIP5, and CMIP6 Climate Models, J. Geophys. Res. Atmos., 125, e2020JD032 701, https://doi.org/10.1029/2020JD032701, 2020.

Hay, S., Priestley, M. D. K., Yu, H., Catto, J. L., and Screen, J. A.: The Effect of Arctic Sea-Ice Loss on Extratropical Cyclones, Geophys. Res. Lett., 50, e2023GL102 840, https://doi.org/10.1029/2023GL102840, 2023.

Hodges, K. I.: A General Method for Tracking Analysis and Its Application to Meteorological Data, Mon. Wea. Rev., 122, 2573–2586, https://doi.org/10.1175/1520-0493(1994)122<2573:AGMFTA>2.0.CO;2, 1994.

Hodges, K. I.: Spherical Nonparametric Estimators Applied to the UGAMP Model Integration for AMIP, Mon. Wea. Rev., 124, 2914–2932, https://doi.org/10.1175/1520-0493(1996)124<2914:SNEATT>2.0.CO;2, 1996.

Hodges, K. I.: Adaptive Constraints for Feature Tracking, Mon. Wea. Rev., 127, 1362–1373, https://doi.org/10.1175/1520-0493(1999)127<1362:ACFFT>2.0.CO;2, 1999.

Hodges, K. I.: TRACK algorithm, https://gitlab.act.reading.ac.uk/track/track, (last access: 27 November 2024), 2020.

Hoskins, B. J., James, I. N., and White, G. H.: The Shape, Propagation and Mean-Flow Interaction of Large-Scale Weather Systems, J. Atmos. Sci., 40, 1595–1612, https://doi.org/10.1175/1520-0469(1983)040<1595:TSPAMF>2.0.CO;2, 1983.

Köhler, D., Räisänen, P., Naakka, T., and Nordling, K.: The future North Atlantic jet stream and storm track: relative contributions from sea ice and sea surface temperature changes; Data and scripts, https://doi.org/10.5281/zenodo.14054331, 2024.

https://doi.org/10.5194/egusphere-2024-3713
Preprint. Discussion started: 13 December 2024

Labe, Z., Peings, Y., and Magnusdottir, G.: Warm Arctic, Cold Siberia Pattern: Role of Full Arctic Amplification Versus Sea Ice Loss Alone, Geophys. Res. Lett., 47, e2020GL088 583, https://doi.org/10.1029/2020GL088583, 2020.

Levine, X. J., Cvijanovic, I., Ortega, P., Donat, M. G., and Tourigny, E.: Atmospheric feedback explains disparate climate response to regional Arctic sea-ice loss, npj Climate and Atmospheric Science, 4, 1–8, https://doi.org/10.1038/s41612-021-00183-w, 2021.

McKenna, C. M., Bracegirdle, T. J., Shuckburgh, E. F., Haynes, P. H., and Joshi, M. M.: Arctic Sea Ice Loss in Different Regions Leads to Contrasting Northern Hemisphere Impacts, Geophys. Res. Lett., 45, 945–954, https://doi.org/10.1002/2017GL076433, 2018.

Naakka, T., Köhler, D., Nordling, K., Räisänen, P., Tronstad Lund, M., Makkonen, R., Merikanto, J., Samset, B. H., Sinclair, V. A., Thomas, J. L., and Ekman, A. M. L.: Polar winter climate change: strong local effects from sea ice loss, widespread consequences from warming seas, manuscript in preparation, 2024.

Notz, D. and Community, S.: Arctic Sea Ice in CMIP6, Geophys. Res. Lett., 47, e2019GL086 749, https://doi.org/10.1029/2019GL086749, 2020.

Oudar, T., Cattiaux, J., and Douville, H.: Drivers of the Northern Extratropical Eddy-Driven Jet Change in CMIP5 and CMIP6 Models, Geophys. Res. Lett., 47, e2019GL086 695, https://doi.org/10.1029/2019GL086695, 2020.

Priestley, M. D. K. and Catto, J. L.: Future changes in the extratropical storm tracks and cyclone intensity, wind speed, and structure, Weather and Climate Dynamics, 3, 337–360, https://doi.org/10.5194/wcd-3-337-2022, 2022.

Priestley, M. D. K., Ackerley, D., Catto, J. L., Hodges, K. I., McDonald, R. E., and Lee, R. W.: An Overview of the Extratropical Storm Tracks in CMIP6 Historical Simulations, J. Climate, p. 6315–6343, https://doi.org/10.1175/JCLI-D-19-0928.1, 2020.

Priestley, M. D. K., Ackerley, D., Catto, J. L., and Hodges, K. I.: Drivers of Biases in the CMIP6 Extratropical Storm Tracks. Part I: Northern Hemisphere, J. Climate, 36, 1451–1467, https://doi.org/10.1175/JCLI-D-20-0976.1, 2023.

Rantanen, M., Karpechko, A. Y., Lipponen, A., Nordling, K., Hyvärinen, O., Ruosteenoja, K., Vihma, T., and Laaksonen, A.: The Arctic has warmed nearly four times faster than the globe since 1979, Communications Earth & Environment, 3, 1–10, https://doi.org/10.1038/s43247-022-00498-3, 2022.

Rivière, G., Berthou, S., Lapeyre, G., and Kageyama, M.: On the Reduced North Atlantic Storminess during the Last Glacial Period: The Role of Topography in Shaping Synoptic Eddies, J. Climate, 31, 1637–1652, https://doi.org/10.1175/JCLI-D-17-0247.1, 2018.

Schemm, S. and Rivière, G.: On the Efficiency of Baroclinic Eddy Growth and How It Reduces the North Pacific Storm-Track Intensity in Midwinter, J. Climate, 32, 8373–8398, https://doi.org/10.1175/JCLI-D-19-0115.1, 2019.

Screen, J. A. and Simmonds, I.: The central role of diminishing sea ice in recent Arctic temperature amplification, Nature, 464, pages 1334–1337, https://doi.org/10.1038/nature09051, 2010.

Screen, J. A., Deser, C., Smith, D. M., Zhang, X., Blackport, R., Kushner, P. J., Oudar, T., McCusker, K. E., and Sun, L.: Consistency and discrepancy in the atmospheric response to Arctic sea-ice loss across climate models, Nature Geoscience, 11, 155–163, https://doi.org/10.1038/s41561-018-0059-y, 2018.

Screen, J. A., Eade, R., Smith, D. M., Thomson, S., and Yu, H.: Net Equatorward Shift of the Jet Streams When the Contribution From Sea-Ice Loss Is Constrained by Observed Eddy Feedback, Geophys. Res. Lett., 49, e2022GL100 523, https://doi.org/10.1029/2022GL100523, 2022.

Simmonds, I. and Li, M.: Trends and variability in polar sea ice, global atmospheric circulations, and baroclinicity, Annals of the New York Academy of Sciences, 1504, 167–186, https://doi.org/10.1111/nyas.14673, 2021.

Simpson, I. R., Shaw, T. A., and Seager, R.: A Diagnosis of the Seasonally and Longitudinally Varying Midlatitude Circulation Response to Global Warming, J. Atmos. Sci., 71, 2489–2515, https://doi.org/10.1175/JAS-D-13-0325.1, 2014.

https://doi.org/10.5194/egusphere-2024-3713
Preprint. Discussion started: 13 December 2024

Smith, D. M., Eade, R., Andrews, M. B., Ayres, H., Clark, A., Chripko, S., Deser, C., Dunstone, N. J., García-Serrano, J., Gastineau, G., Graff, L. S., Hardiman, S. C., He, B., Hermanson, L., Jung, T., Knight, J., Levine, X., Magnusdottir, G., Manzini, E., Matei, D., Mori, M., Msadek, R., Ortega, P., Peings, Y., Scaife, A. A., Screen, J. A., Seabrook, M., Semmler, T., Sigmond, M., Streffing, J., Sun, L., and Walsh, A.: Robust but weak winter atmospheric circulation response to future Arctic sea ice loss, Nature Communications, 13, 727, https://doi.org/10.1038/s41467-022-28283-y, 2022.

Woollings, T., Hannachi, A., and Hoskins, B.: Variability of the North Atlantic eddy-driven jet stream, Quart. J. Roy. Meteor. Soc., 136, 856–868, https://doi.org/10.1002/qj.625, 2010.

Ye, K., Woollings, T., and Screen, J. A.: European Winter Climate Response to Projected Arctic Sea-Ice Loss Strongly Shaped by Change in the North Atlantic Jet, Geophys. Res. Lett., 50, e2022GL102 005, https://doi.org/10.1029/2022GL102005, 2023.

Yu, H., Screen, J. A., Hay, S., Catto, J. L., and Xu, M.: Winter Precipitation Responses to Projected Arctic Sea Ice Loss and Global Ocean Warming and Their Opposing Influences over the Northeast Atlantic Region, J. Climate, 36, 4951–4966, https://doi.org/10.1175/JCLI-D-22-0774.1, 2023.

https://doi.org/10.5194/egusphere-2024-3713
Preprint. Discussion started: 13 December 2024

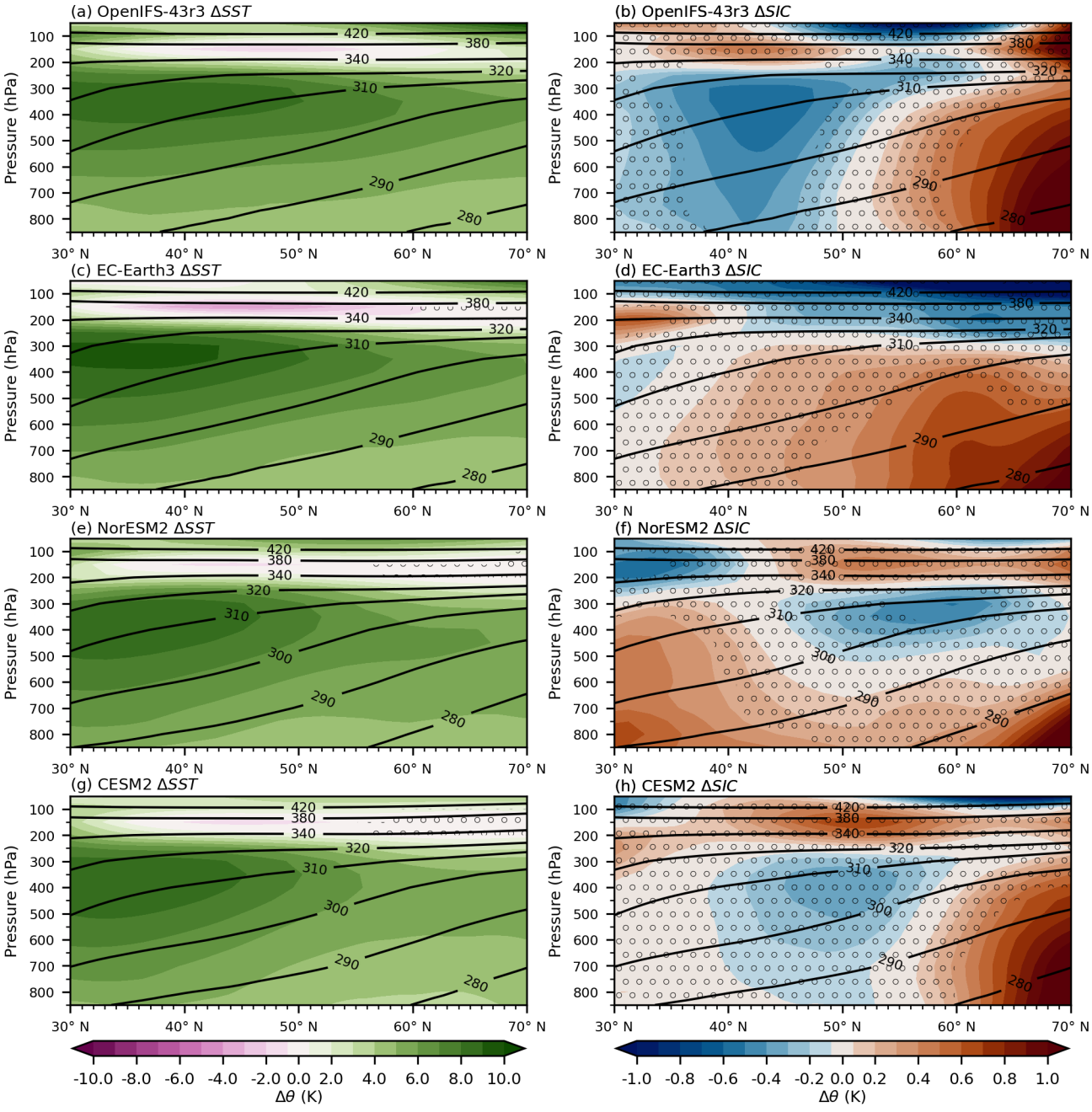

Figure 10. SST response ΔSST (a,c,e,g) and SIC response ΔSIC (b,d,f,h) of the zonal mean (15° W – 35° E) of the 39-year DJF mean of potential temperature θ (in colour shading), the Baseline climatology (in black contours) for (a) & (b) OpenIFS-43r3, (c) & (d) EC-Earth3, (e) & (f) NorEMS2, and (g) & (h) CESM2. Stippling indicates statistically insignificant changes (p-value > 0.05). Note that different colour scales are used because the absolute values of ΔSST and larger than those of ΔSIC.

https://doi.org/10.5194/egusphere-2024-3713
Preprint. Discussion started: 13 December 2024

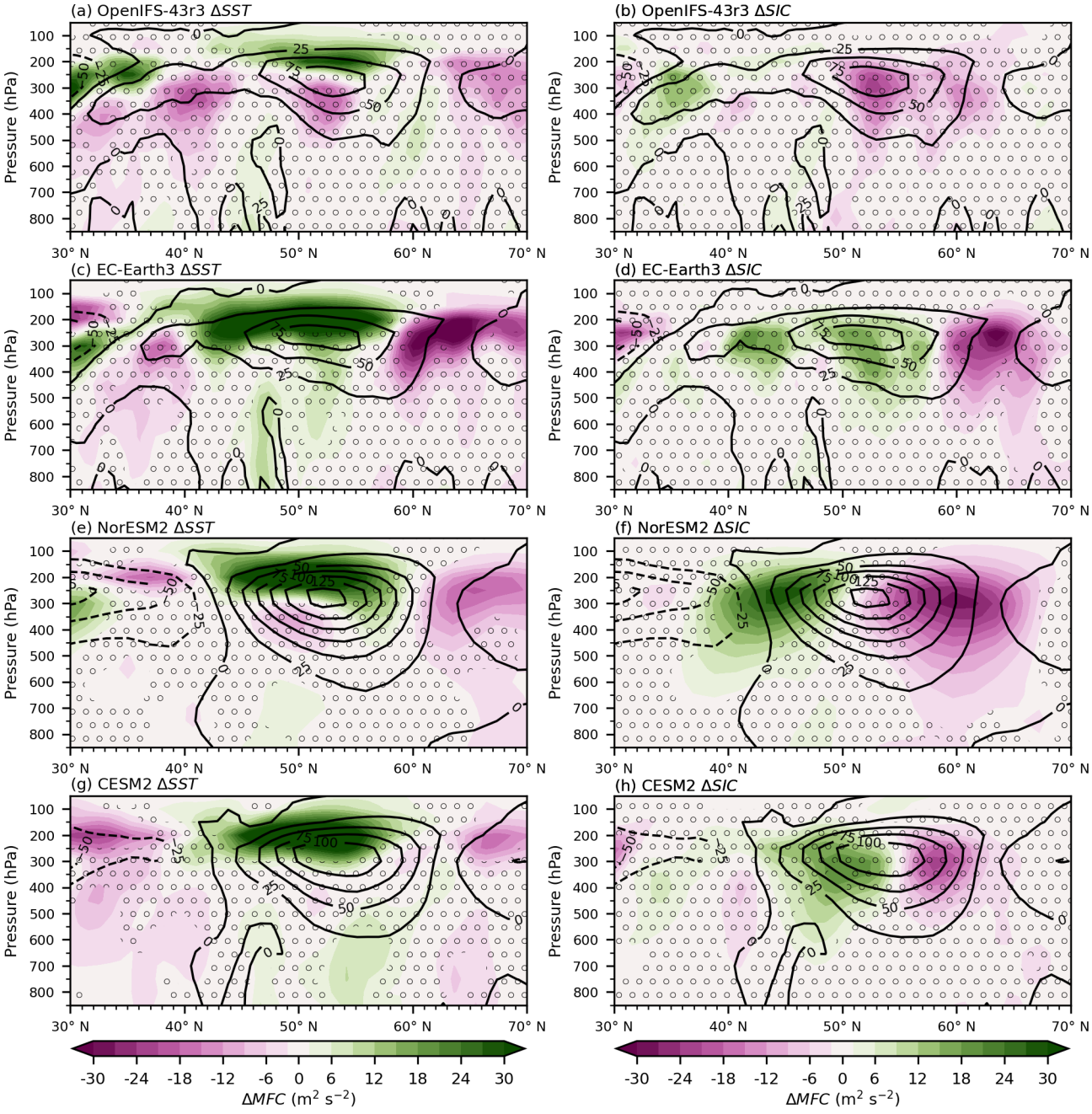

Figure 11. SST response ΔSST (a,c,e,g) and SIC response ΔSIC (b,d,f,h) of the zonal mean (15° W – 35° E) of the 39-year DJF mean of momentum flux convergence MFC (in colour shading), the Baseline climatology (in black contours) for (a) & (b) OpenIFS-43r3, (c) & (d) EC-Earth3, (e) & (f) NorEMS2, and (g) & (h) CESM2. Stippling indicates statistically insignificant changes (p-value > 0.05).

https://doi.org/10.5194/egusphere-2024-3713
Preprint. Discussion started: 13 December 2024

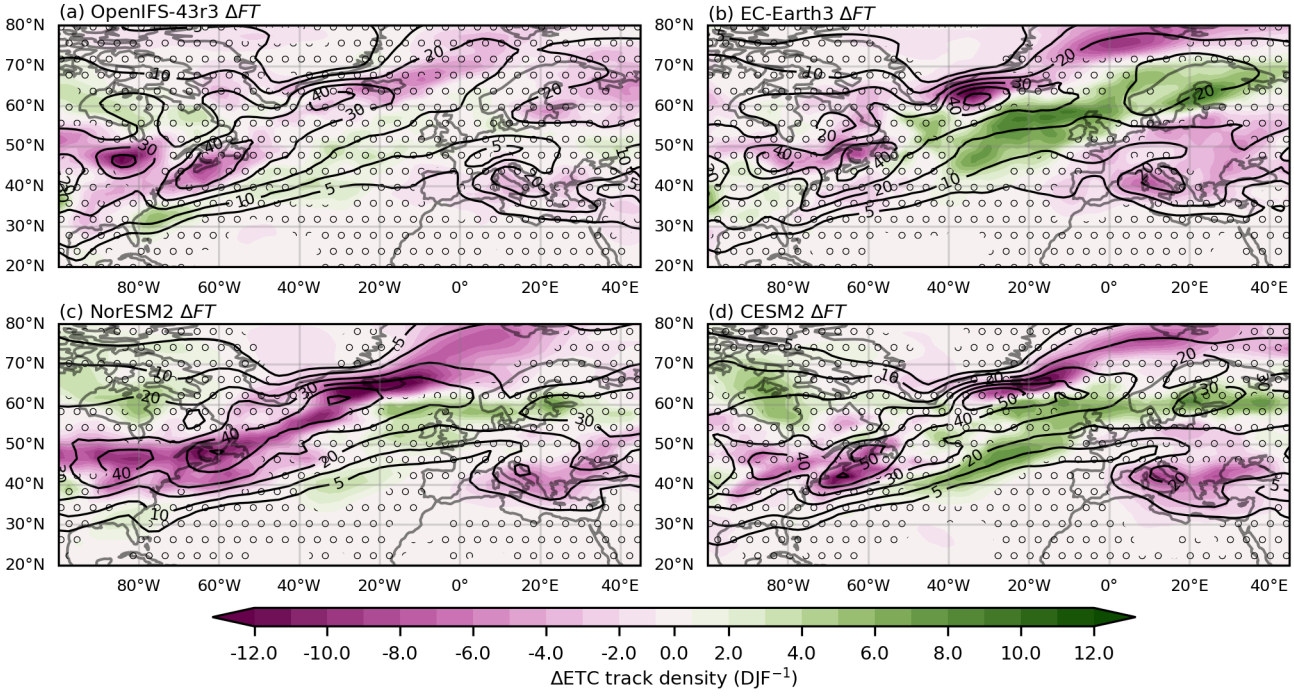

Figure 12. Future response ΔFT of the 39-year DJF mean ETC track density (in colour shading), the Baseline climatology (in black contours) for (a) OpenIFS-43r3, (b) EC-Earth3, (c) NorEMS2, and (d) CESM2. The unit is number of ETCs per 5° spherical cap per winter season (DJF). Stippling indicates statistically insignificant changes (p-value > 0.05).

https://doi.org/10.5194/egusphere-2024-3713
Preprint. Discussion started: 13 December 2024

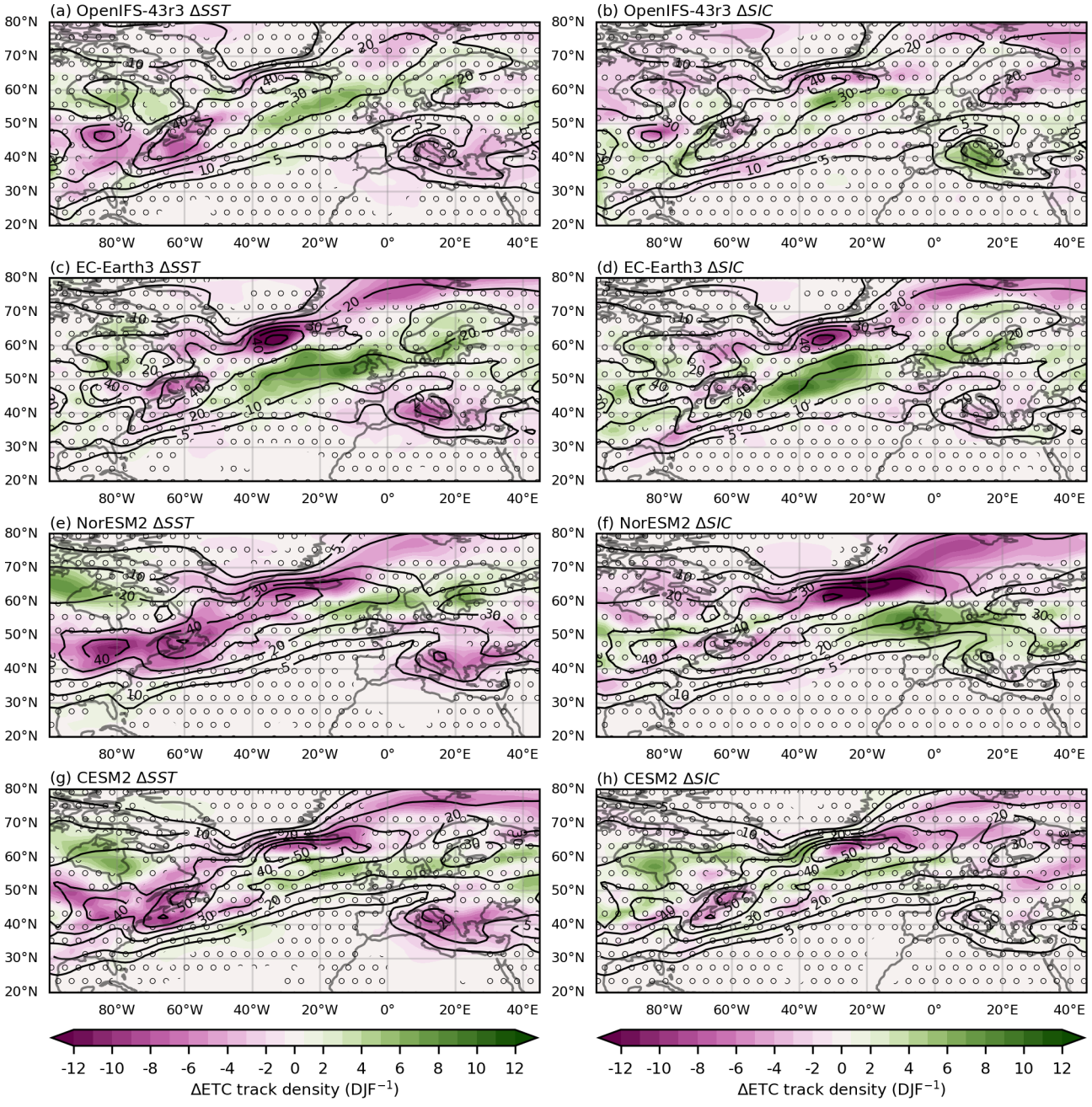

Figure 13. SST response ΔSST (a,c,e,g) and SIC response ΔSIC (b,d,f,h) of the 39-year DJF mean ETC track density (in colour shading), the Baseline climatology (in black contours) for (a) & (b) OpenIFS-43r3, (c) & (d) EC-Earth3, (e) & (f) NorEMS2, and (g) & (h) CESM2. The unit is the number of ETCs per 5° spherical cap per winter season (DJF). Stippling indicates statistically insignificant changes (p-value > 0.05).

https://doi.org/10.5194/egusphere-2024-3713
Preprint. Discussion started: 13 December 2024

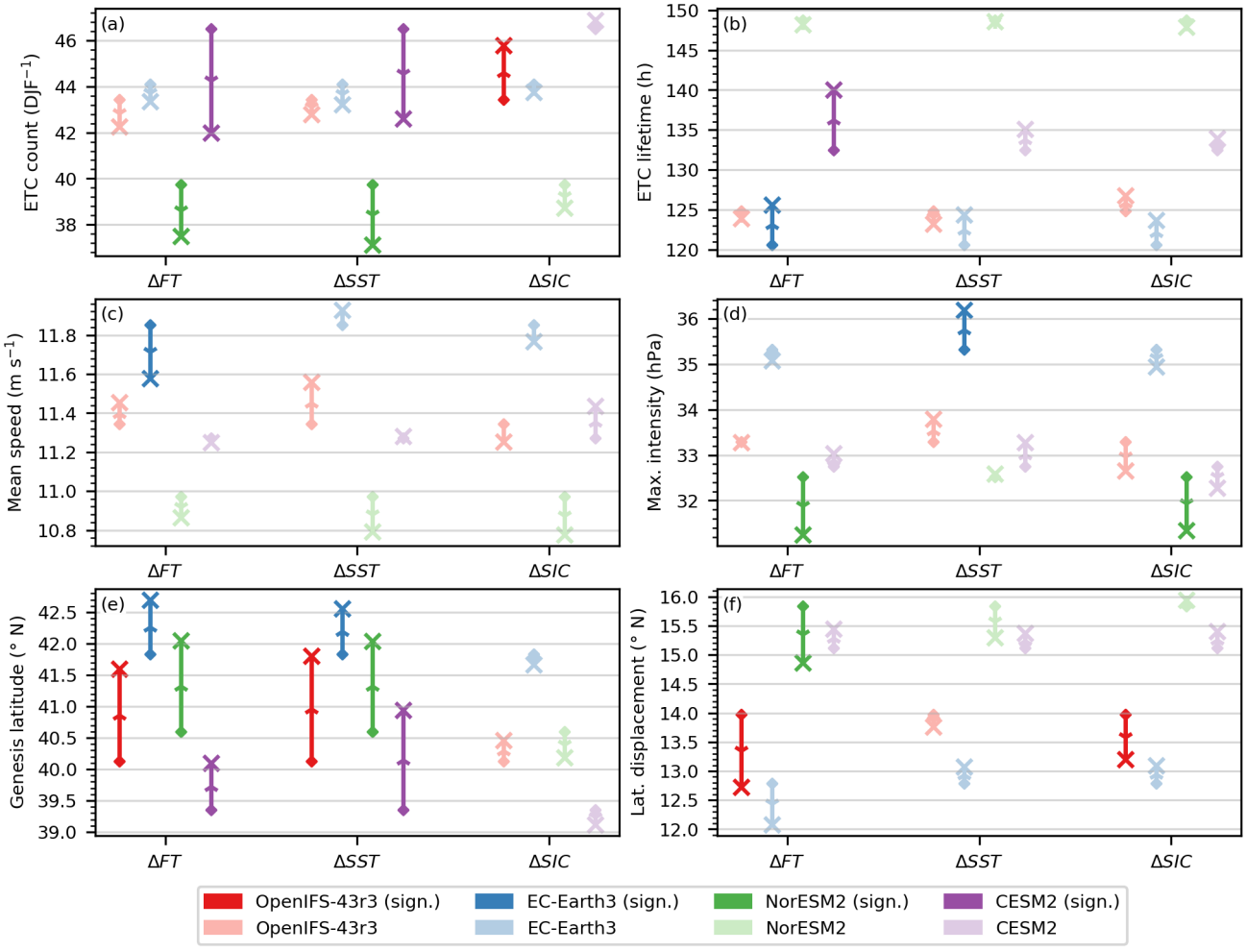

Figure 14. The change in mean values of ETC count per winter season DJF (a), ETC lifetime (b), mean speed (c), maximum intensity (d), genesis latitude (e), and latitudinal displacement (f) for OpenIFS-43r3 (red), EC-Earth3 (blue), NorESM2 (green), CESM2 (purple) with saturated colours indicating statistical significance. Diamonds represent the Baseline simulation and crosses represent the corresponding experiment, respectively. Arrows are added to aid the interpretation of the direction from Baseline to the corresponding experiment.